

โพลีเซลล์สำหรับฟูเรียร์ทรานสฟอร์มอินฟราเรดสเปกโตรมิเตอร์



นายทรงศักดิ์ ทีปกากร

สถาบันวิทยบริการ

วิทยานิพนธ์นี้เป็นส่วนหนึ่งของการศึกษาตามหลักสูตรปริญญาวิทยาศาสตรมหาบัณฑิต

สาขาวิชาเคมี ภาควิชาเคมี

คณะวิทยาศาสตร์ จุฬาลงกรณ์มหาวิทยาลัย

ปีการศึกษา 2543

ISBN 974-13-1354-3

ลิขสิทธิ์ของจุฬาลงกรณ์มหาวิทยาลัย

FLOW CELL FOR FOURIER TRANSFORM INFRARED
SPECTROMETER



Mr. Songsak Tepakakorn

สถาบันวิทยบริการ
จุฬาลงกรณ์มหาวิทยาลัย

A Thesis Submitted in Partial Fulfillment of the Requirements
for the Degree of Master of Science in Chemistry
Department of Chemistry
Faculty of Science
Chulalongkorn University
Academic Year 2000
ISBN 974-13-1354-3

Thesis Title Flow Cell for Fourier Transform Infrared Spectrometer
By Mr. Songsak Tepakakorn
Department Chemistry
Thesis Advisor Sanong Ekgasit, Ph.D.

Accepted by the Faculty of Science, Chulalongkorn University in Partial
Fulfillment of the Requirements for the Master's Degree

.....Dean of Faculty of Science
(Associate Professor Wanchai Phothiphichitr, Ph.D.)

Thesis Committee

.....Chairman
(Associate Professor Sirirat Kokpol, Ph.D.)

.....Thesis Advisor
(Sanong Ekgasit, Ph.D.)

.....Member
(Associate Professor Amorn Petsom, Ph.D.)

.....Member
(Aticha Chaisuwan, Ph.D.)

ทรงศักดิ์ ทีปกากร : โฟลว์เซลล์สำหรับฟูริเยร์ทรานสฟอร์มอินฟราเรดสเปกโตรมิเตอร์
(FLOW CELL FOR FOURIER TRANSFORM INFRARED
SPECTROMETER)

อาจารย์ที่ปรึกษา : อาจารย์ ดร. สนอง เอกสิทธิ์, 81 หน้า. ISBN 974-13-1354-3

งานวิจัยนี้เกี่ยวกับการออกแบบและประดิษฐ์อุปกรณ์เพิ่มเติมแอทเทนนูเอทเตดโทโทลรีเฟลกชันสำหรับการวิเคราะห์ของไหล ด้วยเครื่องเอฟทีไออาร์ สเปกโตรมิเตอร์ โดยอุปกรณ์ใช้ร่วมถูกออกแบบให้มีลักษณะพิเศษที่สามารถวิเคราะห์ของไหล งานวิจัยประกอบด้วยการออกแบบ ประดิษฐ์ ทดสอบการทำงานของอุปกรณ์และเทียบผลการทดลองกับอุปกรณ์ลักษณะเดียวกันที่มีจำหน่ายในเชิงพาณิชย์ เทียบผลการทดลองที่ได้กับทฤษฎีโดยเทียบกับแบบจำลองเชิงสเปกตรัมที่ได้จากการเขียนโปรแกรมคอมพิวเตอร์ จากการศึกษาพบว่ากระจกที่เคลือบด้วยทองสามารถเพิ่มการสะท้อนของแสงได้ดีกว่ากระจกที่ไม่ได้เคลือบด้วยทอง อุปกรณ์ใช้ร่วมที่ประดิษฐ์ขึ้นมีค่าการส่งผ่านพลังงานสูงกว่าอุปกรณ์ลักษณะเดียวกันที่มีจำหน่ายในเชิงพาณิชย์ การวิเคราะห์สารตัวอย่างโดยใช้อุปกรณ์ที่ประดิษฐ์ขึ้นให้สเปกตรัมคล้ายกับการใช้อุปกรณ์ที่มีจำหน่ายในเชิงพาณิชย์ จากผลการทดลองข้างต้นสามารถสรุปได้ว่าอุปกรณ์ที่ประดิษฐ์ขึ้นสามารถใช้ในการวิเคราะห์สารตัวอย่างได้เช่นเดียวกับอุปกรณ์ที่มีจำหน่ายในเชิงพาณิชย์

สถาบันวิทยบริการ
จุฬาลงกรณ์มหาวิทยาลัย

ภาควิชา.....เคมี.....	ลายมือชื่อนิสิต.....
สาขาวิชา...ฟิสิกส์เคมี.....	ลายมือชื่ออาจารย์ที่ปรึกษา.....
ปีการศึกษา...2543.....	ลายมือชื่ออาจารย์ที่ปรึกษาร่วม.....

4172295923 : MAJOR PHYSICAL CHEMISTRY SCIENCE

KEYWORD: FLOW CELL/ ATR/ FT-IR SPECTROMETER

SONGSAK TEPAKAKORN : FLOW CELL FOR FOURIER
TRANSFORM INFRARED SPECTROMETER. THESIS ADVISOR :
SANONG EKGASIT, Ph.D. 81 pp. ISBN 974-13-1354-3.

This research involves design and construction of attenuated total reflection (ATR) accessory for characterization of flowing liquid using FT-IR spectrometer. The new accessory is designed in order to solve the problems of flowing liquid. The research consists of design, construction, and testing of ATR accessory. The results from the constructed accessory were compared with those from commercial accessories. The experimental results were compared with those from spectral simulation. It was found that the energy throughput obtained from the gold-coated reflecting mirror is higher than that from non-gold-coated reflecting mirror. The energy throughput acquired via the constructed accessory is higher than that acquired via the commercial accessories. Spectra acquired via the constructed accessory are similar to those via the commercial accessories. The observed phenomena suggest that the constructed accessory can be employed for characterization of material as commercial accessories.



Department...Chemistry..... Student's signature.....

Field of study...Physical Chemistry..... Advisor's signature.....

A c a d e m i c y e a r C o - a d v i s o r ' s
signature.....

ACKNOWLEDGEMENT

This thesis would never be successfully completed without the excellent advice from my thesis advisor, Dr. Sanong Ekgasit, who always provides me the useful guidance, suggestion, encouragement, and understanding and also patiently practices my technical skill during the whole research.

Gratefully thanks are given to Associate Professor Dr. Sirirat Kokpol, Associate Professor Dr. Amorn Petsom, and Dr. Aticha Chaisuwan for their substantial advice as thesis committee.

I also would like to acknowledge computer and other academic facility supplies from The Austrian-Thai Center (ATC) for computer assisted chemical education and research and instrumental support from Bruker Analytical and Medical Instrument South East Asia.

Finally, I would like to affectionately give all gratitude to my parents for their wholehearted understanding, encouragement, and patient support throughout my entire study.



สถาบันวิทยบริการ
จุฬาลงกรณ์มหาวิทยาลัย

CONTENTS

	Page
ABSTRACT IN THAI.....	iv
ABSTRACT IN ENGLISH.....	v
ACKNOWLEDGEMENT.....	vi
LIST OF FIGURES.....	ix
LIST OF TABLES.....	xiii
LIST OF ABBREVIATIONS.....	xiv
LIST OF SYMBOL.....	xiv
CHAPTER 1 INTRODUCTION.....	1
1.1 Attenuated Total Reflection FT-IR Spectroscopy.....	1
1.2 The ATR Accessory.....	2
1.3 The Objective of Research.....	2
1.4 Scope of Research.....	3
CHAPTER 2 THEORETICAL BACKGROUND.....	4
2.1 Basic Spectroscopy.....	4
2.2 Internal Reflection Spectroscopy.....	6
2.2.1 Interaction of Light and Medium.....	6
2.2.2 Material Characterization by Internal Reflection Spectroscopy.....	10
2.3 Internal Reflection Element.....	11
2.3.1 Aperture.....	12
2.3.2 Number of Reflection.....	14
2.3.3 Various Type of Internal Reflection Element.....	15
2.3.3.1 KRS-5.....	15
2.3.3.2 Silicon and Germanium.....	15
2.3.3.3 Zinc Selenide and Cadmium Telluride.....	16

	Page
2.3.4 Geometry of Internal Reflection Element.....	16
2.3.4.1 Single-Reflection IRE.....	16
2.3.4.2 Multiple-Reflection IRE.....	19
2.4 Internal Reflection Accessory.....	26
2.5 The Limitation of Available Flow Cell ATR Accessory.....	31
 CHAPTER 3 EXPERIMENT.....	 32
3.1 Design and Construction of New Accessory.....	32
3.1.1 Material and Equipment.....	32
3.1.2 Design and Construction.....	32
3.2 Accessory Testing	34
3.2.1 Energy Throughput.....	34
3.2.2 Chemical Testing.....	35
3.2.3 Flowing of liquid.....	36
3.2.4 Spectral Simulation.....	37
 CHAPTER 4 RESULTS AND DISCUSSION	 38
4.1 Design and Construction of Accessory.....	38
4.2 Testing of the accessory.....	41
4.2.1 Energy Throughput.....	41
4.2.2 Chemical Testing.....	54
4.2.3 Flowing of liquid.....	67
 CHAPTER 5 CONCLUSION.....	 68
 REFERENCES.....	 70
 APPENDIX.....	 71
 CURRICULUM VITAE.....	 81

LIST OF FIGURES

Figures	Page
2.1 Propagation of a linearly polarized electromagnetic wave in the direction of propagation.....	5
2.2 Interaction of light with matter.....	5
2.3 Path of the radiation impinges at the interface between two media.....	7
2.4 Conditions under which total internal reflection occurs. Light travels from an optically denser medium and impinges at the surface of the optically rarer medium ($\eta_1 > \eta_2$).....	8
2.5 Reflectivity versus angle of incidence for an interface between media with indices, $\eta_1 = 4.0$ and $\eta_2 = 1.33$, for light polarized perpendicular and parallel to plane of incidence.....	9
2.6 Single-pass internal reflection element showing path of light, defining aperture A, length l, and thickness t of IRE.....	12
2.7 Calculated angular dependence of aperture for an internal reflection plate.....	13
2.8 Schematic illustration of single-pass IRE (a) Single-pass parallelepiped plate (b) Single-pass trapezoidal plate.....	14
2.9 Triangular prism with a fixed angle of incidence.....	16
2.10 Hemicylindrical prism with variable angle of incidences.....	17
2.11 Hemispherical prism with variable angle of incidence.....	18
2.12 Fixed-angle, single-pass, multiple internal reflection plates (a) trapezoid (b) paralleled with $\theta < 45^\circ$ (c) thin plate with $\theta > 45^\circ$	19
2.13 Double-pass multiple internal reflection plate.....	21
2.14 Schematic diagram of a horizontal double-pass internal reflection plate.....	21
2.15 Double-pass plate with single aperture and cocked end.....	22
2.16 Schematic diagram of light path in the vertical double-pass multiple plate.....	23
2.17 Geometrical construction of vertical double-pass plate.....	24
2.18 Single-pass variable angle, multiple internal reflection plates.....	25

Figures	Page
2.19 Double-pass variable angle, multiple internal reflection plates	25
2.20 Fixed-angle internal reflection attachment employing Ge trapezoid plate, $\theta = 45^\circ$ for a double-beam instrument.....	28
2.21 Fixed-angle internal reflection attachment employing Ge parallelepiped plate, $\theta = 45^\circ$ for a double-beam instrument.....	28
2.22 Fixed-angle multiple reflection attachment (ATR-4).....	29
2.23 Fixed-angle multiple reflection attachment market by Wilks Scientific Corp. (a) optical layout (b) Photograph showing unit mounted in spectrometer with fiber sample prepared for analysis.....	29
2.24 Schematic diagram of the horizontal ATR laboratory reactor.....	30
2.25 Schematic diagram of the low pressure horizontal ATR flow cell.....	31
3.1 Illustration of new constructed accessory	33
3.2 The optical diagram of the constructed accessory.....	33
4.1 (A) the constructed accessory. (B) the constructed accessory equipped with 30° angle of incidence (C) the constructed accessory equipped with 45° angle of incidence (D) the constructed accessory equipped with 60° angle of incidence	39
4.2 Photograph of the Baseline HATR equipped with Single-pass trapezoidal germanium plate.....	40
4.3 Photograph of the Seagull™.....	40
4.4 (A) Interferogram and (B) single beam spectra of air acquired via the 45° constructed accessory before the reflecting mirror is coated with gold.....	43
4.5 (A) Interferogram and (B) single beam spectra of air acquired via Baseline HATR accessory.....	44
4.6 (A) Interferogram and (B) single beam spectra of air acquired via the 45° constructed accessory after the reflecting mirror is coated with gold.....	45
4.7 (A) Interferogram and (B) single beam spectra of air acquired via the Seagull™ accessory.....	46

Figures	Page
4.8 (A) Interferogram and (B) single beam spectra of air acquired via the 30° constructed accessory before the reflecting mirror is coated with gold.....	48
4.9 (A) Interferogram and (B) single beam spectra of air acquired via the 30° constructed accessory after the reflecting mirror is coated with gold.....	49
4.10 (A) Interferogram and (B) single beam spectra of air acquired via the 45° constructed accessory before the reflecting mirror is coated with gold.....	50
4.11 (A) Interferogram and (B) single beam spectra of air acquired via the 45° constructed accessory after the reflecting mirror is coated with gold.....	51
4.12 (A) Interferogram and (B) single beam spectra of air acquired via the 60° constructed accessory before the reflecting mirror is coated with gold.....	52
4.13 (A) Interferogram and (B) single beam spectra of air acquired via the 60° constructed accessory after the reflecting mirror is coated with gold.....	53
4.14 ATR spectra of nujol acquired via (A) The Baseline HATR (B) The Seagull™ (C) The constructed accessory after the reflecting mirror is coated with gold at 45° angle of incidence.....	57
4.15 ATR spectra of nujol acquired via (A) The Seagull™ at 30° angle of incidence. (B) The constructed accessory after the reflecting mirror is coated with gold at 30° angle of incidence.....	58
4.16 ATR spectra of nujol acquired via (A) The Seagull™ at 60° angle of incidence. (B) The constructed accessory after the reflecting mirror is coated with gold at 60° angle of incidence.....	59
4.17 ATR spectra of nujol acquired via the constructed accessory after the mirror was coated with gold equip with (A) 30° angle of incidence (B) 45° angle of incidence (C) 60° angle of incidence.....	60

Figures	Page
4.18 ATR spectra of nujol between 2200-2000 cm^{-1} at 45° angle of incidence (A) Baseline HATR (B) Seagull™ (C) constructed accessory.....	61
4.19 ATR spectra of nujol of the constructed accessory between 2200-2000 cm^{-1} (A) 30° (B) 45° (C) 60°.....	62
4.20 ATR spectra of nujol of the Seagull™ between 2200-2000 cm^{-1} (A) 30° (B) 45° (C) 60°.....	63
4.21 p/s ratio (A) Baseline HATR (B) constructed accessory 45° angle of incidence (C) Seagull 45° angle of incidence.....	64
4.22 p/s ratio (A) Seagull 30° angle of incidence (B) constructed accessory 30° angle of incidence.....	65
4.23 p/s ratio (A) Seagull 60° angle of incidence (B) constructed accessory 60° angle of incidence.....	66
4.24 Experimental setup for study flow system.....	67

LIST OF TABLES

Tables	Page
4.1 Dimensions and Number of reflections of Internal Reflection Element (IRE) in Attenuated Total Reflection (ATR) accessories.....	56



สถาบันวิทยบริการ
จุฬาลงกรณ์มหาวิทยาลัย

LIST OF ABBREVIATIONS

ATR	: attenuated total reflection
N	: number of reflection
A	: aperture
FT-IR	: Fourier transform infrared
Ge	: germanium
IRE	: internal reflection element
IRS	: internal reflection spectroscopy
HATR	: horizontal attenuated total reflection
SSP	: single-pass parallelepiped
SST	: single-pass trapezoidal
KRS-5	: thallium iodide-thallium bromide
ZnSe	: zinc selenide

LIST OF SYMBOL

η	: reflective index
--------	--------------------

สถาบันวิทยบริการ
จุฬาลงกรณ์มหาวิทยาลัย

CHAPTER 1

INTRODUCTION

1.1 Attenuated Total Reflection (ATR) FT-IR Spectroscopy

Optical spectroscopy is one of the most powerful and widely employed analytical techniques. Spectra of small samples can be recorded with optical spectroscopic techniques. One of the most powerful techniques is attenuated total reflection Fourier transform infrared (ATR FT-IR) spectroscopy. When the light strikes an interface between media of two different refractive indices, reflection and refraction occur. The light beam has angle of reflection equal angle of incidence. According to Snell's law, when refractive index of the first media is higher than that of the second media and the angle of incidence equals the critical angle, total internal reflection is observed. In ATR, the sample is placed in contact to the internal reflection element (IRE). The IRE is a material with a high refractive index such as zinc selenide (ZnSe) and germanium (Ge). Generally, the infrared beam is focused onto the beveled edge of IRE by a set of mirror, reflected through the IRE, and then directed to the detector by another set of mirrors. The electric field penetrates a short distance into the sample. The evanescent wave is absorbed by the sample. ATR FT-IR technique measures the interaction of the evanescent wave and the sample. The observed spectrum is the characteristic of the sample. However, the spectrum will depend on several parameters such as the angle of incidence, the sample size (thickness and area), the wavelength of the radiation, and the number of reflections.

Since ATR FT-IR technique is nondestructive, simple to operate, reliable, and provides information directly related to chemical structure, the technique becomes a routine technique in laboratory.

1.2 The ATR Accessory

N. Wright and R. Barnes invented the infrared spectrometer (IR) in 1930. They showed that the infrared spectrometer can be use for both qualitative and quantitative analyses. In 1962, Connecticut Instrument Corporation constructed the ATR accessory. Later on, several commercial firms such as Barnes Engineering, Beckman Instruments, Inc., Perkin-Elmer Corp., Pike Technology, Spectra Tech., and Harrick Scientific Corp. have developed various ATR accessories for specific and demanding applications. Some of their instruments will be shown in chapter 2.

The commercial accessories have several configurations depending on sample form, angle of incidence, and specific experimental setup. Such as the Baseline HATR, the horizontal IRE is equipped with accessory. The different configuration of accessory also depends on shape of IRE. Since the available IRE in our laboratory is single-pass parallelepiped germanium plates. The design and configuration of the accessory with depend on shape of available IRE.

1.3 The Objective of This Research

Due to the available ATR liquid cell has several limitation especially when it is employed for fluid or flowing liquid of which properties change as a function of time. The accessory must be imported form foreign country. Thus the accessory itself is expensive. The objective of this research is to construct a new attenuated total reflection accessory with low cost, easy operation and applicable for flowing liquid. Moreover, the new accessory can be applied for characterization of solid sample as well.

1.4 Scope of Research

1. To design and construct ATR flow cell accessory.
2. To determine the energy throughput of the constructed accessory and compare the results with available commercial accessories.
3. To determine the ATR spectra of liquid sample via the constructed accessory and compare the results with those from commercial accessories.
4. To determine angle accuracy of the constructed accessory by comparison of the observed spectra with those obtained via spectral simulation.



สถาบันวิทยบริการ
จุฬาลงกรณ์มหาวิทยาลัย

CHAPTER 2

THEORETICAL BACKGROUND

2.1 Basic Spectroscopy

Spectroscopy is a scientific discipline concerned with the interactions of electromagnetic radiation with matter. When the electromagnetic radiation impinges on the surface of an object, interactions between the incident beam and the molecules will alter the incident radiation. The incident beam can be reflected, scattered, transmitted, or absorbed by the matter. Since a spectroscopic experiment allows detection of reflected, scattered, transmitted, or absorbed light, it needs a source of light an object of study, and a suitable detector. Thus, change in the electromagnetic radiation by the matter carries information about the chemical composition or physical properties of the matter.

While an object and a detector are defined by specific chemical and physical properties, light needs further consideration. Light is an electromagnetic wave. In its simplest monochromatic form, light can be represented as oscillating electric and magnetic fields that propagate in space (shown in Figure 2.1). The electric and magnetic vectorial components are orthogonal to each other and to the direction of propagation.

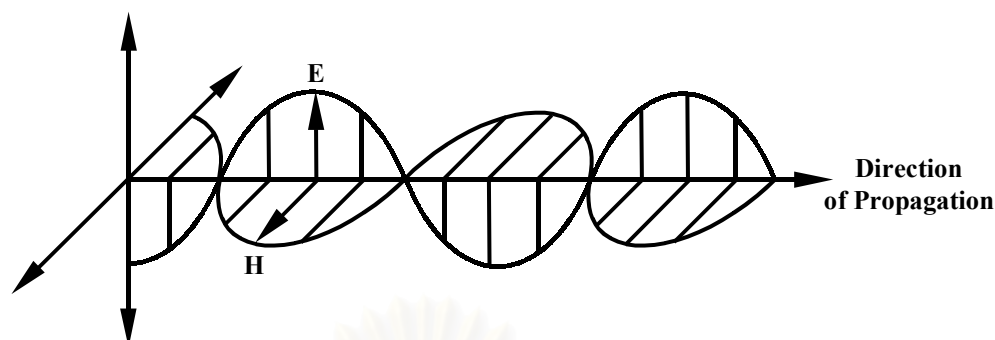


Figure 2.1 Propagation of a linearly polarized electromagnetic wave in the direction of propagation.

When such an electromagnetic radiation impinges on a specimen, ray of the incident beam may be reflected, scattered, transmitted, or absorbed depending on the experimental arrangement. The total amount of incident energy is the sum of reflected, scattered, transmitted, and absorbed light. A schematic illustration for an interaction between light and matter is illustrated in Figure 2.2. This process can be expressed by the following relationship.

$$I_0 = I_R + I_S + I_T + I_A \quad (2.1)$$

Where I_0 is the intensity of the incident beam and I_R , I_S , I_T and I_A are the reflected, scattered, transmitted, and absorbed beams, respectively. The intensity of each beam depends on the intensity and wavelength of the incident beam, the optical properties of the specimen, the concentrations of species, and the geometry of the experimental setup.

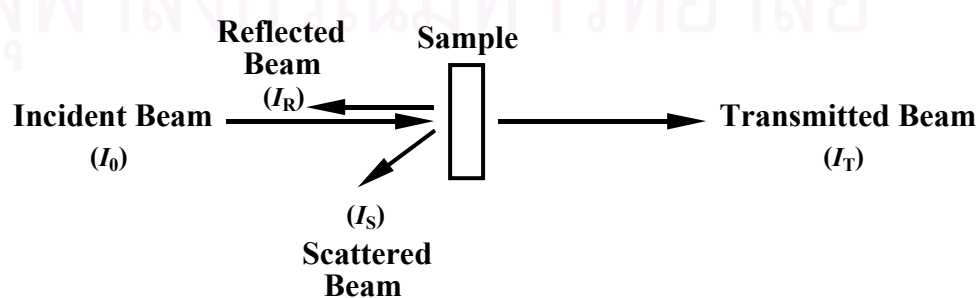


Figure 2.2 Interaction of light with matter.

Let's consider the electromagnetic radiation when a sample is inserted between a source of light and a detector. The sample absorbs a fraction of the incident radiation. In order to measure the region and amount of light being absorbed by the sample, the ratio of the sample attenuated intensity (I) and nonattenuated intensity (I_0) of the radiation is required. The ratio can be quantitatively related to the chemical composition of the sample by the Beer-Lambert law [1] as:

$$\frac{I_0}{I} = e^{-A(\nu)} = e^{-c \varepsilon(\nu) l} \quad (2.2)$$

where $A(\nu)$ is the sample absorbance at a given wavenumber ν , c is the concentration of the absorbing functional group, $\varepsilon(\nu)$ is the wavenumber-dependent absorption coefficient, and l is the film thickness for the IR beam at a normal incidence.

2.2 Internal Reflection Spectroscopy

2.2.1 Interaction of light and medium

When electromagnetic radiation strikes an interface between two media with different refractive indices, the beam will be partially reflected and partially transmitted at the interface. The transmitted beam is refracted within the second medium as shown in Figure 2.3. The law that governs the reflection process requires that the angle of incidence equals the angle of reflection. In this case, reflection is specular. If electromagnetic radiation passes from one medium to another that has a different refractive index, a sudden change of beam direction is detected because of the difference in propagation velocity through two media. If light propagates through a medium with refractive index η_1 and enters a medium with refractive index η_2 (see Figure 2.3), the light path will change, the relationship between the angle of the incident radiation and that of the refracted radiation is given by the following relationship [1]:

$$\frac{\sin \theta_1}{\sin \theta_2} = \frac{\eta_2(\nu)}{\eta_1(\nu)} \quad (2.3)$$

where θ_1 and θ_2 are the angle of incidence and the angle of refraction, respectively.

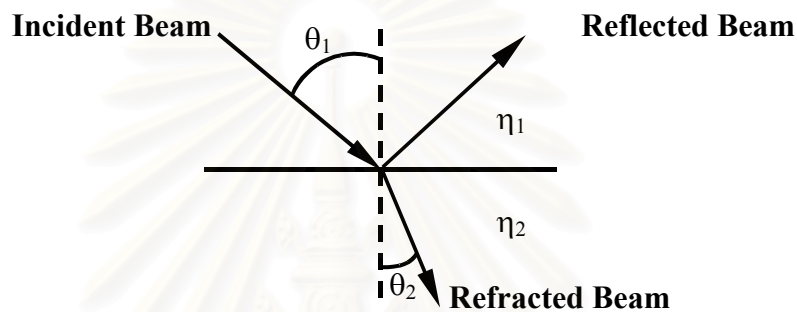


Figure 2.3 Path of the radiation impinges at the interface between two media.

The reflected amplitude for unit of incoming beam, under parallel and perpendicular polarization are given, respectively, by Fresnel's equations:

$$r_{\perp} = - \frac{\sin(\theta_2 - \theta_1)}{\sin(\theta_2 + \theta_1)} \quad (2.4)$$

$$r_{\parallel} = \frac{\tan(\theta_2 - \theta_1)}{\tan(\theta_2 + \theta_1)} \quad (2.5)$$

Perpendicular polarization is also known as TE (transverse electric) or s (senkrecht) waves. Parallel polarization is also known as TM (transverse magnetic) or p (parallel) waves [2].

Total internal reflection occurs when light traveling in an optically denser medium impinges on surface of an optically less dense medium (i.e., $\eta_1 > \eta_2$) with an incident angle greater than the critical angle. The critical angle can be derived from Snell's law. The critical angle can be given in terms of refractive indices as shown in

equation 2.6. According to Figure 2.4, when the angle of incidence equals the critical angle, θ_c , the refracted angle equals 90° . This implies that under a total internal reflection condition there is no light from the optically denser medium travels across the interface into the optically rarer medium.

$$\theta_c = \sin^{-1}\left(\frac{\eta_2}{\eta_1}\right) \quad (2.6)$$

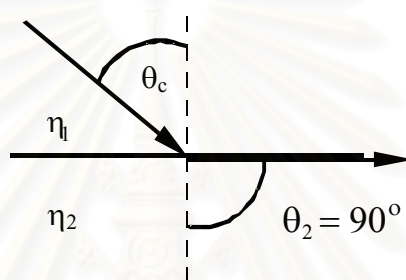


Figure 2.4 Conditions under which total internal reflection occurs. Light travels from an optically denser medium and impinges at the surface of the optically rarer medium ($\eta_1 > \eta_2$).

Both p-polarized beam and s-polarized beam become totally reflected when the angle of incidence greater than or equal the critical angle. The reflectivities for internal reflection can be calculated from equations 2.4 and 2.5. The plot between reflectivity and angle of incidence is shown in Figure 2.5.

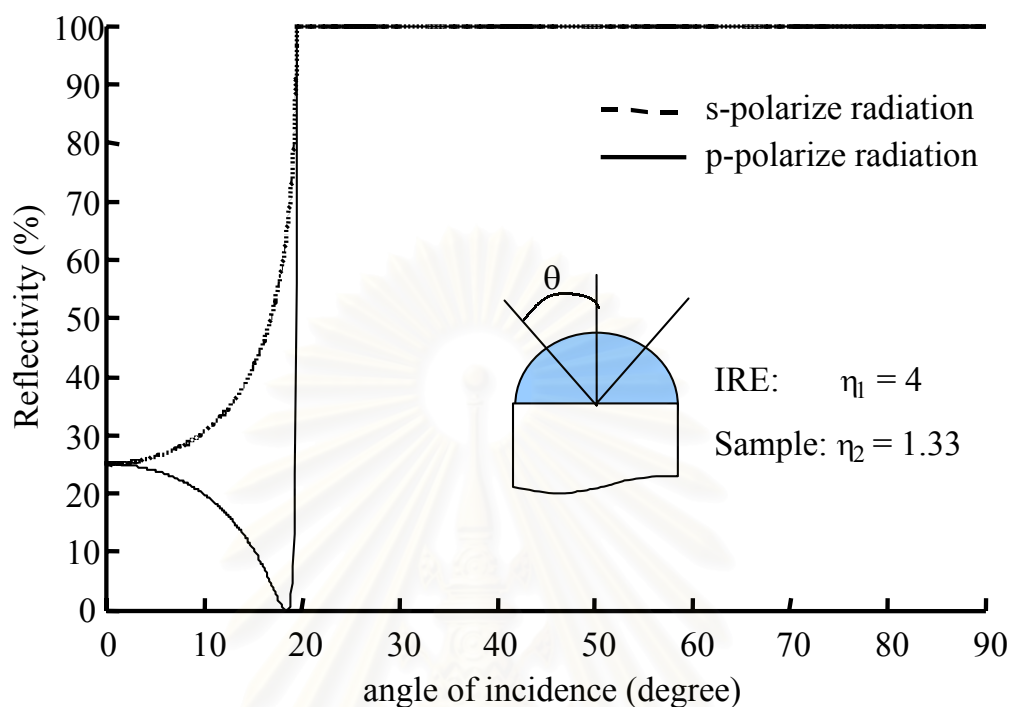


Figure 2.5 Reflectivity versus angle of incidence for an interface between media with indices, $\eta_1 = 4.0$ and $\eta_2 = 1.33$, for light polarized perpendicular and parallel to plane of incidence.

Total Internal reflection spectroscopy is, therefore, a technique of recording the optical spectrum of a sample material that is in contact with an optically denser medium. The wavelength dependence of the reflectivity of this interface is measured by introducing light into the denser medium. In this technique the reflectivity is a measure of the interaction of the electric field with the material and the resulting spectrum is also a characteristic of the material. Since the technique complements conventional optical absorption techniques and can be used in some instances where conventional technique cannot readily be applied. The areas of application of optical spectroscopy are, thus, extended.

2.2.2 Material Characterization by internal reflection spectroscopy

Internal reflection spectroscopy (IRS) is a nondestructive sampling technique for obtaining an infrared spectrum of material, which is either too thick, or strongly absorbing to be analyzed by more traditional transmission methods. Samples examined by IRS generally require minimal or no sample preparation.

ATR FT-IR spectroscopy stand for Attenuated Total Reflection Fourier Transform Infrared Spectroscopy. It is a material characterization technique using an internal reflection principle. The sample is placed in contact against a crystal with high refractive index, such as zinc selenide (ZnSe: $n=2.4$), thallium iodide-thallium bromide (KRS-5: $n=2.4$), or germanium (Ge: $n=4.0$). The infrared beam from an infrared source is passed through the IRE, which is interact with sample at the interface and then directed to the detector. The infrared path is controlled by a set of reflecting mirrors.

Attenuated total reflection spectrum is due to an absorbing coupling mechanism whereby the reflectivity for total internal reflection can be continuously adjusted between some value greater than 0 (e.g., 40%) and 100% by placing an absorbing medium in contact with the reflecting surface of the crystal. The resulting reflection is said to be attenuated; the energy is absorbed and is not transmitted but may, for example, be converted to heat. Attenuated total reflection is observed when the angle of incidence is set and remains above the critical angle and the wavelength is swept through absorption bands.

The unusual characteristics associated with total internal reflection is beneficial in many areas. Those applications include precision measurements of angles and refractive indices; the construction of beam splitters, optical filters, laser cavities, light modulators, light deflector, and the measurement of film thickness.

2.3 Internal Reflection Elements (IRE)

The internal reflection element (IRE) is the transparent optical element used in internal reflection spectroscopy for establishing the conditions necessary to obtain internal reflection spectra of materials. Radiation is propagated through the IRE by means of total internal reflection. The sample is placed in contact with the reflecting surface. The ease of obtaining an internal reflection spectrum and the information obtained from the spectrum are determined number of characteristics of the IRE. A choice must be made in the working angle or range of angle of incidence, number of reflections, aperture, number of passes, surface preparation, and material from which it is made [2]

For internal reflection spectroscopy the information obtained is deduced from the deviation of the reflectivity from unity by:

$$R = 1 - a \quad (2.7)$$

where a is the absorption parameter. The contrast of the spectrum increases as effective thickness increases. Largest effective thicknesses are obtained by selecting the lowest possible refractive index for the IRE and working at the smallest angle of incidence. Because of distortion of spectra and other practical considerations, there is an upper limit to effective thickness. The contrast of the spectrum can then be enhanced by employing multiple reflections. The relationship between reflectance and absorption parameter under multiple reflection is given by:

$$R = (1 - a)^N \quad (2.8)$$

Where N is number of reflections. When a is small, the above equation can be rewritten as:

$$R \cong 1 - Na \quad (2.9)$$

2.3.1 Aperture

The index of refraction of any material changes with wavelength. Therefore, the degree of refraction at the entrance face of the IRE, hence the internal angle of incidence, θ , on the sampling surface is wavelength dependent for oblique incidence. Since it is desirable to maintain the same angle of incidence over the entire wavelength range under investigation, refraction should be eliminated. This is the case when the light enters and leaves the IRE via the aperture at normal incidence. Normal incidence on the apertures also eliminates changes of polarization of the light beam by the IRE. The entrance and exit faces of the IRE are thus specially shaped or beveled, for example, as shown in Figure 2.6.

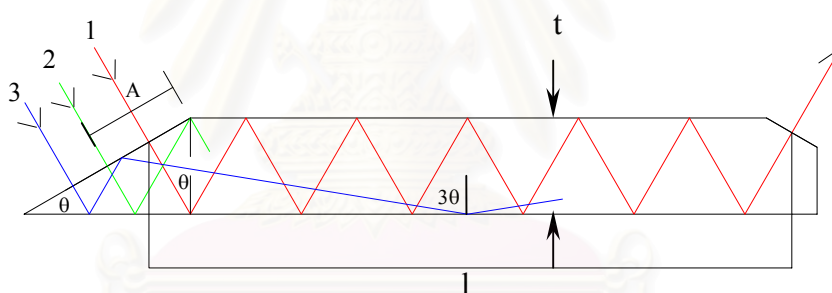


Figure 2.6 Single-pass internal reflection element showing path of light, defining aperture A , length l , and thickness t of IRE.

The entire area of the entrance and exit faces does not always serve as “useful” aperture. This is clearly demonstrated by ray 3 which is reflected internally from the beveled face before it enters the plate. The internal angle of incidence for this ray on the sampling surface for the second reflection is increased by 2θ , making it 3θ inside the IRE instead of θ as desired.

The aperture of the IRE is thus defined as that portion of the beveled area, which can be utilized to conduct the light into the IRE at the desired angle of

incidence θ . The aperture is equal to the total area of the beveled face for angles of incidence of 45° or greater and is given by

$$A = t \csc \theta \quad (2.10)$$

For angles less than 45° only part of the bevel contributes to the useful aperture and this is given by

$$A = 2t \sin \theta \quad (2.11)$$

Figure 2.7 show plot of aperture against the angle of incidence. The aperture rises from zero at normal incidence to a maximum at 45° where it has a value of 1.414 times the plate thickness, t , and then decreases to a value equal to the plate thickness at grazing incidence.

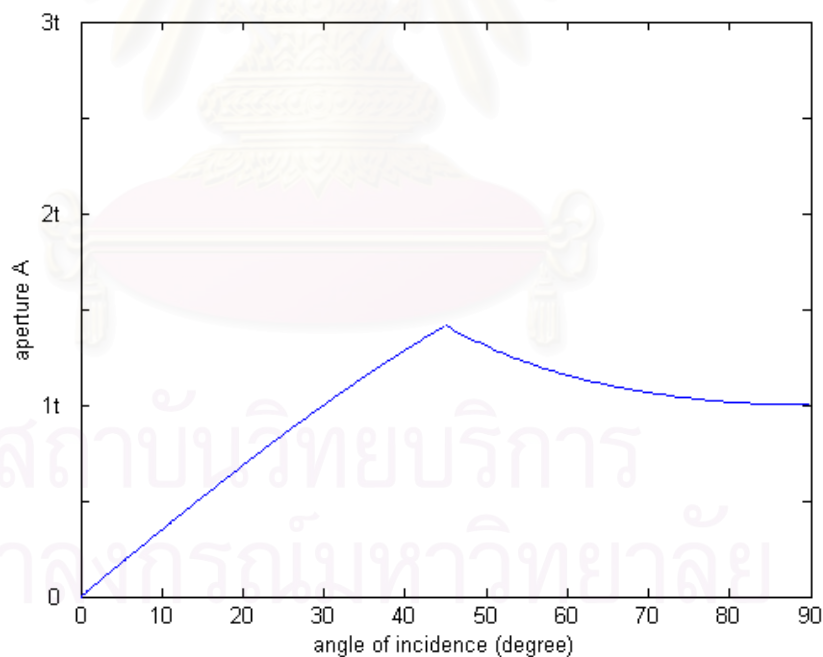


Figure 2.7 Calculated angular dependence of aperture for an internal reflection plate.

For $\theta \leq 45^\circ$ the entire area of the broad surfaces is sampled when the total aperture, as defined by equation 2.11, is illuminated. For $\theta > 45^\circ$, however, the

distance between consecutive reflections along the broad surface, i.e., “skip distance,” is greater than the projection of the aperture on the broad surface (i.e., beam width on broad surface) and hence the entire area of the broad surfaces is not sampled. For $\theta > 45^\circ$ the aperture can be increased from that given by equation 2.10 to that given by equation 2.11 by “trumpeting” the end of the plate, and then the entire area of the broad surface is sampled when the total aperture is illuminated.

2.3.2 Number of reflection (N)

The number of reflections is calculated from simple geometrical considerations. The beam advances with a distance (“skip distance”) of $t \tan(\theta)$ for each reflection. If the dimension of an internal reflection element (IRE) is given by its length (l), width (w), and thickness (t). The length of the IRE, measured from the center of the entrance aperture to the center of the exit aperture, the total number of reflections for a single pass in the plate is given by

$$N = (l/t) \cot \theta \quad (2.12)$$

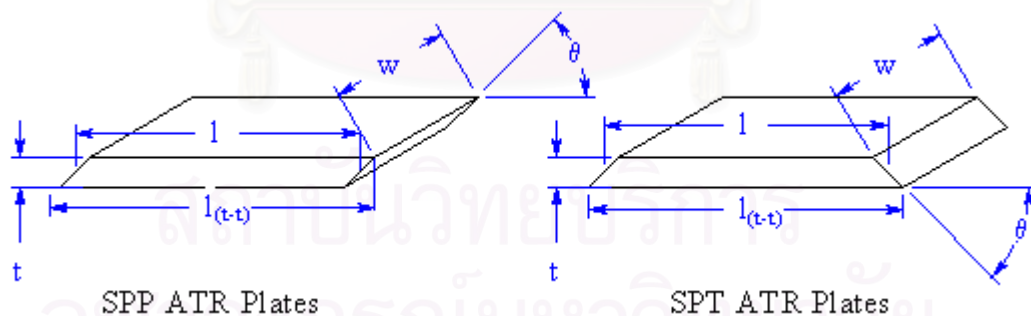


Figure 2.8 Schematic illustration of single pass IRE a) single-pass parallelepiped plate (SPP) IRE b) single-pass trapezoidal plate (SPT) IRE.

N is zero for grazing incidence. It increases for decreasing θ , and rises sharply for small angles as θ decreases further.

2.3.3 Various type of Internal Reflection Element

Several properties of some commonly used IRE are considered in the selection of appropriate crystal such as refractive index, durability, spectral range coverage, chemical inertness, and price. Additionally, once the material has been chosen, the geometry of the IRE such as shape, angle of incidence, and dimension, must also be defined. Angle of incidence and dimension define the number of reflections of the IRE. As the intensity of an internal reflection spectroscopy spectrum is proportional to the number of reflections, IRE allowing multiple reflections are generally employed. However, the shape of the IRE is generally dictated by the type of accessory to be used [3].

2.3.3.1 KRS-5

KRS-5 is one of the most commonly used materials as an IRE. It is also comparatively inexpensive. It has a spectral range comparable to that exhibited by most transmission methods when the crystal is new. However, the material is rather soft and easily deformed. The spectral range decreases gradually with use and the appearance of scratches on the polished faces. Repolishing of the scratched surface is possible. Thallium compounds are toxic, and although the IRE itself is not harmful in normal usage, the dust from polishing is quite poisonous. The ductility of the crystal's surface is beneficial in establishing a good contact with the sample and, thus, the acquisition of good quality spectra.

2.3.3.2 Silicon and Germanium

Silicon and germanium are good choices of IRE when the samples to be examined are strongly scattering or possess high refractive index. Since the crystals have high refractive index, the depth of penetration is lower than that of KRS-5. One drawback with these IREs is their limited spectral range (9500-1500 cm^{-1} for silicon and 5000-900 cm^{-1} for germanium).

2.3.3.3 Zinc Selenide and Cadmium Telluride

For applications where germanium is too fragile and KRS-5 is easily scratched during sample examination, ZnSe ($20000\text{-}700\text{ cm}^{-1}$) or cadmium telluride ($10000\text{-}350\text{ cm}^{-1}$) can be good candidate although they are relatively expensive. Their refractive index and spectral range coverage are similar to KRS-5 ($14000\text{-}400\text{ cm}^{-1}$). As a result, they provide good quality full mid-infrared spectra range.

2.3.4 Geometry of Internal Reflection Elements

The geometry of the internal reflection IRE determines the ease of the internal reflection spectroscopy techniques can be employed to a particular sample [Appendix A]. Some have been designed to simplify instrumentation while others have been designed with the nature of the sample in mind, e.g., whether the sample is liquid, powder, or thin film. However, IRE may be identified by its shape and dimension [2].

2.3.4.1 Single-Reflection IRE

Single-reflection IRE can be used to record spectra of bulk materials in which the absorption is sufficiently strong and in which adequate contact to the sample, e.g., liquids, pliable solids, and samples with smooth surfaces.

2.3.4.1.1 Fixed-angle IRE

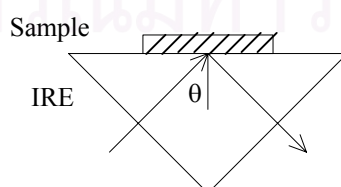


Figure 2.9 Triangular prism with a fixed angle of incidence.

The simplest of all internal reflection elements is the triangular prism (shown in Figure 2.9), where the light beam enters and leaves at normal incidence. The IRE is operated at a fixed angle of incidence. Prisms can be prepared for various angle of incidence or facets may be provided on a single prism so that it might be operated at a few selected angles. The solid sample is placed in contact with the reflecting surface and its spectrum is acquired. For liquid samples, a suitable cell has to be built in order to hold the liquids.

2.3.4.1.2 Variable-angle IRE's

1. Hemicylindrical IRE

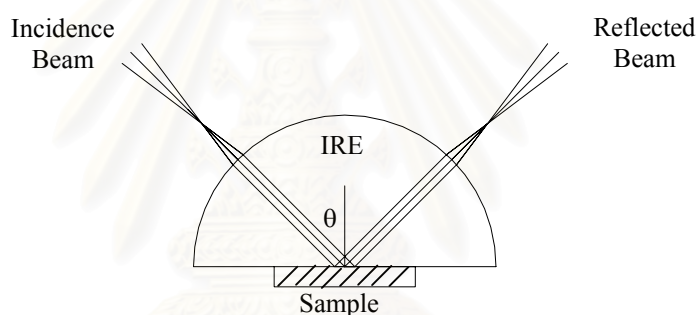


Figure 2.10 Hemicylindrical prism with variable angle of incidence.

The hemicylindrical prism, (shown in Figure 2.10) was first used by Fahrenfort as the IRE. It is the simplest variable-angle IRE. The hemicylinder must be carefully aligned so that its axis is parallel to the monochromator slit. By bringing the light beam to a focus at a distance in front of the curved surface, the light beam is, in the first approximation, collimated within the hemicylinder parallel to the slit but not perpendicular to it. The light beam is refocused at the same distance from the surface when it leaves the IRE. The distance is given in terms of the refractive index and radius of the prism by:

$$d = \frac{r}{\eta_1 - 1} \quad (2.13)$$

Here r is the radius of the hemicylindrical prism and η_1 the refractive index of the prism.

The hemicylinder is useful for measuring optical constants where a carefully selected angle of incidence is essential. The possibility of changing the angle of incidence is also useful in controlling the contrast of the spectrum.

For small samples, minute quantities, and solid samples where contact to the reflecting surface is not easily achieved, it is desirable to condense the beam size at the reflecting surface. This can be done by condensing the beam and bringing it to a focus at the reflecting surface of the hemicylinder. Collimation of the beam, however, is then not obtained. The beam can be condensed to some extent and collimation can be partially preserved by employing a hemicylinder with small radius. It is evident from equation 7 that the distance d will be reduced and the beam width at the reflecting surface will therefore also be reduced. Collimation of the beam within the hemicylindrical prism, however, degenerates because of the finite width of the slit image and large angular spread of the beam

2. Hemispherical IRE

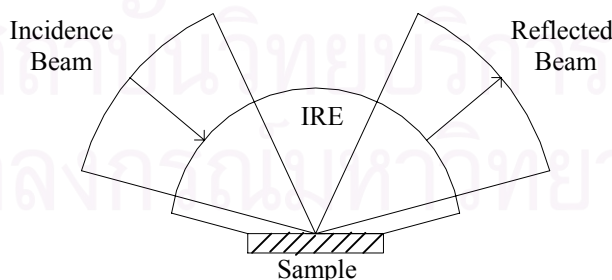


Figure 2.11 Hemispherical prism with variable angle of incidence.

The bottom section is cone-shaped to facilitate the contacting the between material to the sampling surface. The use of a hemispherical IRE resembles to the condensing systems as that in conventional transmission. The use of a hemispherical

IRE with a strongly converging beam definitely enhances the sensitivity for examining minute quantities. The gain in sensitivity however does not increase as rapidly as the beam area is reduced. The reason for this is that in order to produce a small spot size a highly converging beam is required which, in turn, means that a large range of angles of incidence must be employed.

2.3.4.2 Multiple-Reflection IRE

For many bulk materials, thin films, and particularly monomolecular layers, spectra of sufficient contrast cannot be obtained using a single reflection IRE. A multiple reflection IRE must be employed in order to enhance the contrast. A variety of IRE's have been developed for this purpose and some geometrics are particularly suited for certain applications. Because of simplicity of construction and ease of determining and maintaining a given angle of incidence it is desirable to reflect the light internally from plane, parallel surfaces.

2.3.4.2.1 Fixed-Angle Multiple Reflection Plates

Single Pass Plate

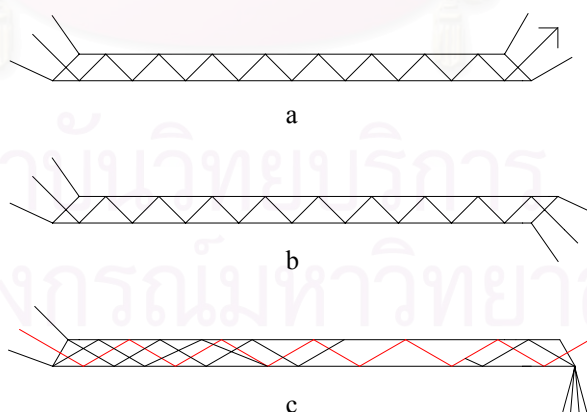


Figure 2.12 Fixed-angle, single-pass, multiple internal reflection plates (a) trapezoid (b) paralleled with $\theta < 45^\circ$ (c) thin plate with $\theta > 45^\circ$.

The simplest and most commonly used multiple internal reflection element is the single-pass plate shown in Figure. 2.12. It may be in the form of either a trapezoid or parallelepiped. Here the light is introduced into the plate via the entrance aperture, is propagated down the length of the plate via multiple internal reflections from the opposing flat surfaces, and leaves via the exit aperture. As was pointed out earlier, the number of reflections is directly proportional to the length of the plate and the cotangent of the angle of incidence and inversely proportional to its thickness. As many as five hundred reflections have been employed. It is impractical to make the plates longer than 10 cm and thinner than 0.25 mm. This places a rough upper limit of 10^3 reflections for this type of IRE.

For single-pass plates a distinction is made between thin and thick plates. For thin plates the light is focused upon the entrance aperture and will entirely fill it. The light is then contained within the plate by the two large flat areas and will illuminate the entire exit aperture and leave the plate with the same beam spread. Both entrance and exit apertures act as focal points and there is no change in the width of the source image regardless of the length of the plate. The light rays will be completely mixed within the plate if it is sufficiently long. The light rays need not be traced through the plate, it is only necessary to focus the light source on the entrance aperture and focus the exit aperture on the spectrometer slit when the IRE is placed in the sampling space of commercial spectrometers. Equivalently, when the IRE is placed in the monochromatic beam after the exit slit, it is necessary to focus the spectrometer slit image on the entrance aperture of the IRE and focus the exit aperture on the detector element. It should be realized that for $\theta > 45^\circ$, because the skip distance exceeds the projected beam area on the broad surface, the light does not initially fill the entire plate even when the total aperture is illuminated as shown in Figure 2.12c. For a divergent beam, however, the light will tend to fill the entire plate as it traverses the length of the plate. Therefore some of the light will approach the exit aperture from the wrong direction and be totally reflected by this aperture and be lost even when the exit aperture is placed at the correct location for the central ray (as shown in Figure 2.12c).

Double-Pass Plate

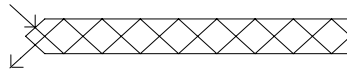


Figure 2.13 Double-pass multiple internal reflection plate.

In double-pass plate the light beam enters an aperture at one end and is propagated via multiple total reflection down the length of the plate just as in the single-pass plate. However, it is totally reflected at the other end, from a surface perpendicular to the two large flat areas. At the complement of the angle of incidence on the broad faces and returns via a similar path to exit from the plate through an aperture adjacent to the entrance aperture (as shown in Figure 2.13). The Double-pass plates simplify optical alignment since the entrance and exit beams have a common focal point while the single-pass plates have two focal points. For a given length of plate the number of reflections is increased by a factor of 2 over the single-pass plate, thus, it represents a folded system. The total aperture however (entrance plus exit) is constant and therefore each aperture has been reduced by a factor of two compared to the single-pass plate, when the exit and entrance apertures are of the same area. An important advantage of the double-pass plates is that one end of the plate is free and it can be dipped into a liquid or powder to acquire spectrum (as shown in Figure 2.14).

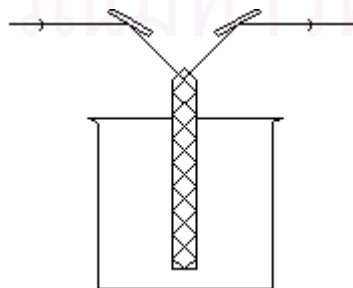


Figure 2.14 Schematic diagram of a horizontal double-pass internal reflection plate.

Another important application of the double-pass plates is their use in evacuated systems since only one optical window is now required to bring the beam in and out of a vacuum system.

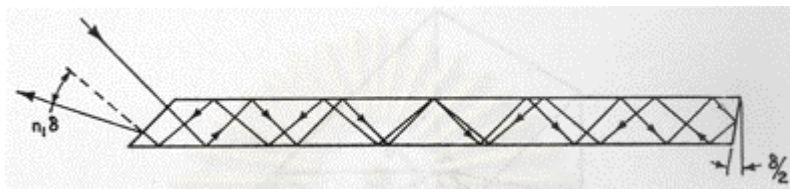


Figure 2.15 Double-pass plate with single aperture and cocked end.

A variation of the double-pass plate is one with a single bevel at one end and a cocked end-reflecting surface, as shown in Figure 2.15. In this case the same aperture is employed for both the entrance and exit beams. If the light beam strikes the entrance aperture at normal incidence it is propagated down the length in the usual manner. After it strikes the end surface its angle of incidence on the broad faces for the return path is changed by twice the angle of the tilt, viz., δ (plus or minus depending on the direction of the tilt). The beam will return and strike the entrance aperture at non-normal incidence, and therefore the exit beam will be refracted away from the entrance beam by approximately $n_1\delta$ degrees, as shown in Figure 2.15.

Vertical Double-Pass Plate.

For the double-pass plate (as shown in Figure 2.14), with the aid of the necessary additional optical components to reorient the slit images, could be placed in a vertical position and then easily dipped into liquids and powders to record their spectra. This horizontal double-pass plate can be converted into a vertical one, thereby eliminating the need of the additional optical components, by making a 45° diagonal cut and beveling the long edge as shown in Figure 2.16. If the appropriate surfaces are polished, light entering one face of the beveled edge will propagate horizontally by internal reflection until it strikes the diagonal surface. It is then deflected downwards, where it is propagated by means of multiple internal reflection.

From the two opposing broad surfaces, until it strikes the bottom surfaces. Here it is totally reflected, returns via a similar path and is reoriented to a horizontal path after striking the diagonal cut, is propagated horizontally via internal reflection, and exits from the other beveled edge.

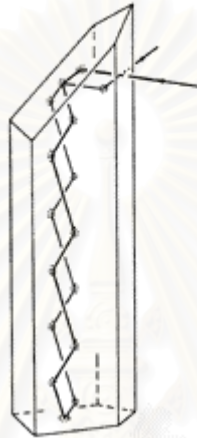


Figure 2.16 Schematic diagram of light path in the vertical double-pass multiple plate.

The vertical double-pass plate is not restricted to an angle of incidence of 45° but, provided the 45° diagonal plane is maintained, the range of angles of incidence that can be employed is the same as for the horizontal double-pass plate, viz., from the critical angle θ_c to $(90^\circ - \theta_c)$. Thus it is possible to use it at other angles of incidence or to construct a variable angle, vertical double-pass internal reflection element by providing a cylindrical entrance aperture. This can be proved mathematically and is also evident from the geometrical construction shown in Figure 2.17.

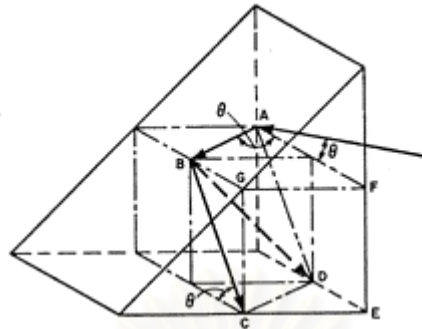


Figure 2.17 Geometrical construction of vertical double-pass plate.

2.3.4.2.2 Variable-Angle Multiple Reflection Plates

In many instances where multiple reflection IRE's must be employed it is still necessary to be able to vary the angle of incidence. These include the measurement of optical constants, the study of the interaction of the evanescent wave with the absorbing rarer medium and many cases where it is necessary to record spectra of optimum contrast. Therefore, there is a need for variable-angle multiple reflection IRE. A variety of variable-angle multiple reflection internal reflection elements have been employed to date one designed for a few reflections and others for an indefinite number of reflections.

The constructions discussed here apply to thick and thin plates. For thick plates it is necessary to trace the ray within the IRE and therefore, although a wide range of angles can be obtained, the angle of incidence cannot be varied continuously unless the length of the plate is changed. This is also partially true for thin plates where maximum transmission is obtained when the central rays pass through the focal points of the system.

1. Single-Pass IRE.

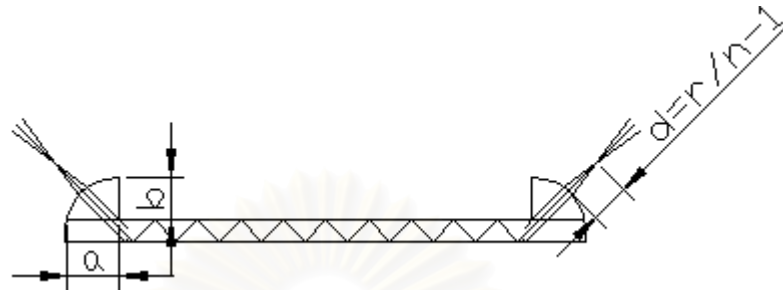


Figure 2.18 Single-pass variable angle, multiple internal reflection plates

A variable-angle single-pass multiple internal reflection element can be constructed by placing “quarter rounds” on a plate, as shown in Figure 2.18. In this case, the quarter round may be optically contacted to the plate or the entire structure may be molded from a suitable material. The “quarter round” must be cut in such a way that the center of curvature is located at a point midway in the plate. Thus the dimension b is roughly equal to $(a - t/2)$. The focusing condition for collimation within the IRE discussed earlier can be applied here. The quarter round for the exit beam may be located anywhere along the length of the plate, depending on the number of reflections required. Furthermore, it may be located on the same side of the plate or the opposite side.

2. Double-Pass.

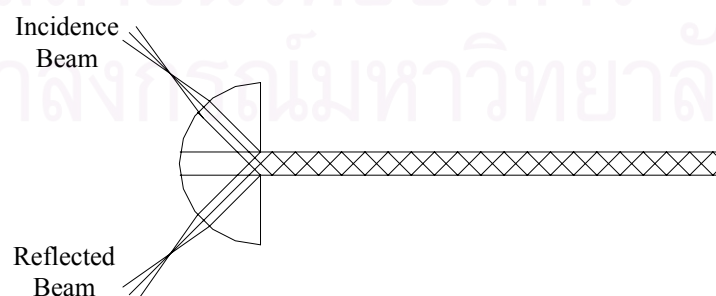


Figure 2.19 Double-pass variable angle, multiple internal reflection plates.

A double-pass multiple IRE can obviously be constructed in the same manner as the single-pass one. In this case, however, the “quarter rounds” are placed opposite each other at the same end of the plate. In addition to the possibility of varying the angle of incidence continuously, all of the advantages of the double-pass plate apply to this structure. A schematic diagram of a variable-angle, double-pass plate is shown in Figure 2.19.

2.4 Internal Reflection Accessory

In general, adequate instrumentation for internal reflection spectroscopy was not commercially available before 1965 which hampered its early development. A number of workers developed their own instrumentation; but many others who did not want to embark upon an instrumentation program shelved their ideas—at least temporarily. The requirements of internal reflection spectrometers include the ability to vary easily the angle of incidence over a wide range, readily accessible IRE's, and adequate space for auxiliary equipment such as polarizers, vacuum or heating chambers.

Instrumentation for internal reflection spectroscopy can be developed in one of four ways, all based on the use of existing commercial spectrometers. These are as follow;

1. The use of special IRE's which do not substantially displace or defocus the light beam at the entrance slit and therefore can be placed in the existing sampling space of a conventional spectrometer without employing additional optical components.
2. The developments of special attachments utilizing transfer optics, which can also be inserted in the sampling space with no disturbance of the optical alignment.

3. The development of completely new layouts for the source optics of the spectrometer which will include the necessary components for internal reflection measurements.

4. The extraction of the monochromatic beam from the monochromator.

In most of the spectrometers in use, double-beam operation is employed. Double-beam operation is more sensitive than single-beam because, with the resulting flat base line, higher amplifications can be employed and then source fluctuations and atmospheric absorption bands are cancelled to a high degree. For a high degree of balancing, it is necessary that the same portion of the infrared source contributes to both beams to ensure identical spectral compositions. For internal reflection, surface roughness of the IRE contributes to unbalance. Equal lengths of optical material should be traversed by both the reference and sample beams to compensate for any absorptions by the optical material e.g., due to lattice vibrations and free carriers.

Some of the commercial accessory will be discussed in the following sections.

1. Trapezoid Plates in Double-Beam Layout

The accessory has developed and employed the layout shown in Figure 2.20. The light path is initially folded using mirrors and retro-mirror and brought to a focus at one end of a fixed-angle (45°) multiple reflection Ge plate in the form of a trapezoid. The exit beam is refocused and directed to the entrance slit of the monochromator. A sample was usually placed on both sides of the IRE.

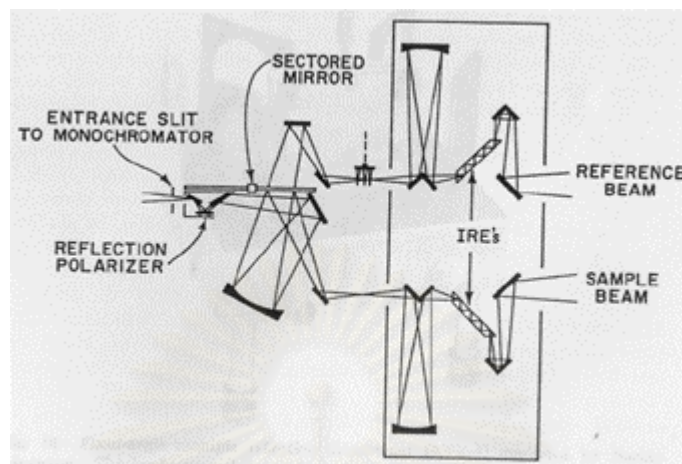


Figure 2.20 Fixed-angle internal reflection attachment employing Ge trapezoid plate, $\theta = 45^\circ$ for a double-beam instrument.

2. Parallelepiped Plates in Double-Beam Layout

Sharpe of Bell Telephone Laboratories, Murray Hill, New Jersey has converted his double-beam spectrometer for internal reflection work in the manner shown in Figure 2.21. Initially he employed 8-reflection Ge plates in the form of parallelograms at $\theta = 45^\circ$. He later modified the system to accept internal reflection plates with 30 reflections.

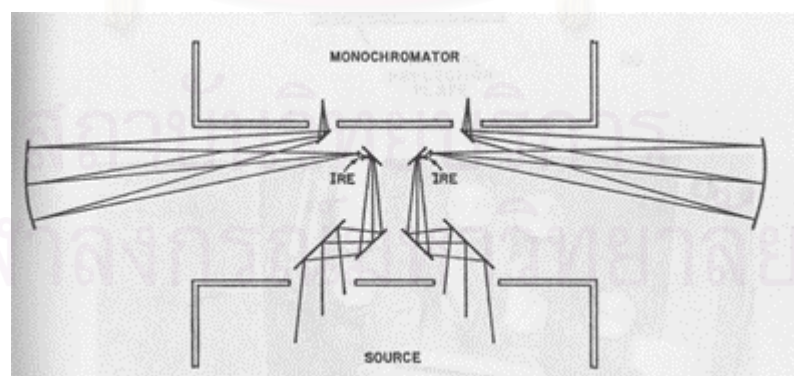


Figure 2.21 Fixed-angle internal reflection attachment employing Ge parallelepiped plate, $\theta = 45^\circ$ for a double-beam instrument.

3. Commercial Attachments for Trapezoid Plates

Barnes Engineering, Perkin-Elmer, and Wilks Scientific supply fixed-angle multiple internal reflection attachments which may be placed in the sampling space of commercial spectrometers. The optical layout and photographs of a unit (ATR-4) marketed by Barnes Engineering is shown in Figure 2.22. The optical layout and photograph of another attachment, marketed by Wilks Scientific is shown in Figure 2.23a and 2.23b, respectively. The photograph shows how it is mounted in the sampling space of a commercial spectrometer with a fiber sample pressed against the IRE.

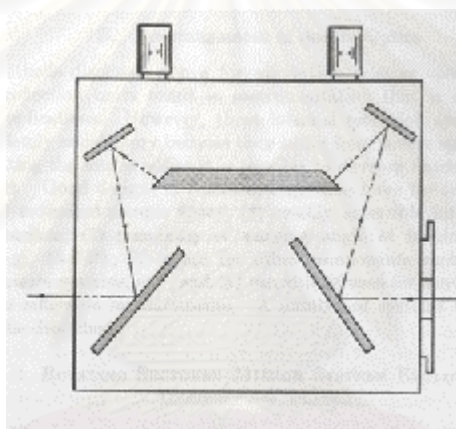


Figure 2.22 Fixed-angle multiple reflection attachment (ATR-4).

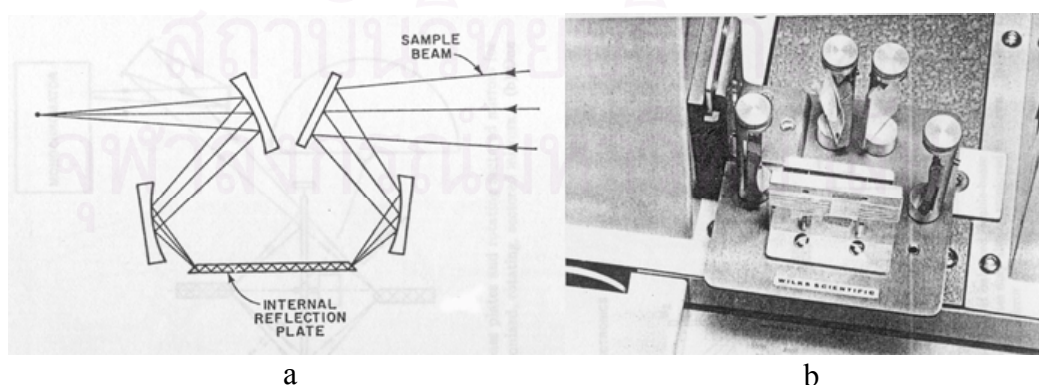


Figure 2.23 Fixed-angle multiple reflection attachment market by Wilks Scientific Corp. (a) optical layout (b) Photograph showing unit mounted in spectrometer with fiber sample prepared for analysis.

4. The Horizontal ATR Laboratory Reactor

The stirred reactor used for reaction monitoring is shown in Figure 2.24 [5]. The horizontal ATR crystal is mounted in the bottom plate of the reactor. The low pressure horizontal ATR reactor can be used for monitoring the reactions. The reactor content can be well stirred during the reaction.

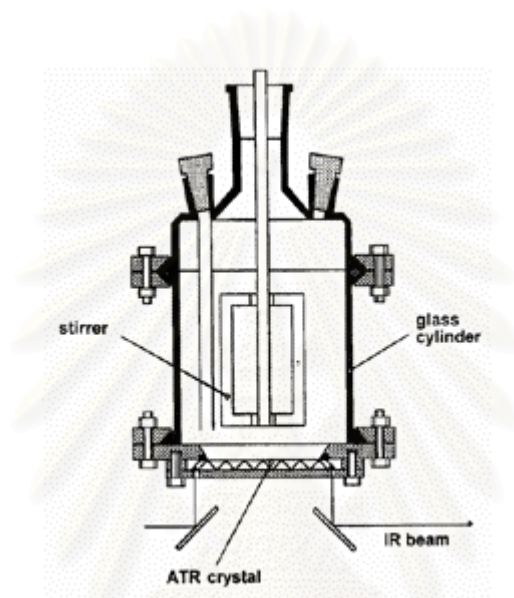


Figure 2.24 Schematic diagram of the horizontal ATR laboratory reactor.

The ATR crystal is sealed against the liquid within the reactor by elastomeric seal. In order to avoid absorption peaks due to the seal the upper flat side of the ATR crystal is coated with gold where the seal touches the crystal. The ATR crystal can be changed by loosening the metal plate at the lower side of the ATR crystal.

5. Low Pressure horizontal ATR Flow Cell

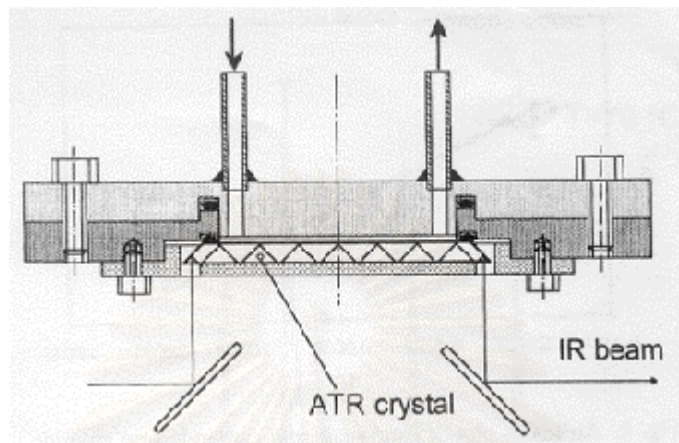


Figure 2.25 Schematic diagram of the low pressure horizontal ATR flow cell.

The flow cell was used for reaction monitoring in a bypass in built analogous to the low pressure ATR reactor and is shown in Figure 2.25[5]. The ATR crystal is sealed by an elastomer and can be changed. The wet side of the ATR crystal can be cleaned easily after loosening only four screws and opening the ATR flow cell.

2.5 The Limitation of Available Flow Cell ATR Accessory

Since the commercial ATR liquid cell has several limitation especially when it is employed for fluid or flowing liquid which properties change as a function of time. Due to the Internal Reflection Element (IRE) is aligned in horizontal or vertical configuration, the pump is used to assist flow of liquid sample. But the pump is caused to pressure build-up and sample mixing within the liquid cell. Therefore, the experimental result may be mistake. Furthermore, the commercial ATR accessories are expensive, which must be imported from abroad. The commercial accessories are difficult to repair or modify for specific experiment due to complex.

CHAPTER 3

Experiment

3.1 Design and Construction of New Accessory

3.1.1 Materials and equipments

1. Aluminium
2. Mechanical tools
3. Milling machine
4. Lathe
5. Reflecting mirror

3.1.2 Design and Construction

The schematic illustration of the newly designed attenuated total reflection (ATR) accessory is shown in Figure 3.1. The body of the accessory was made of aluminium. The accessory can be adjusted to three angle of incidence: 30° , 45° and 60° for different experimental requirement and type of the internal reflection element (IRE). The angle can be changed by rotating the sample holder. The ATR internal reflection element was aligned with inclined angle for free flow of fluid on IRE. The sample inlet and outlet are big enough to avoid pressure build up within the accessory. The reflecting mirror was gold-coated Ni-Co-Al alloy. The mirror holder can be adjusted for different plate IRE. The IRE is a single-pass parallelepiped (SPP) germanium plate ($50 \times 10 \times 2$ mm).

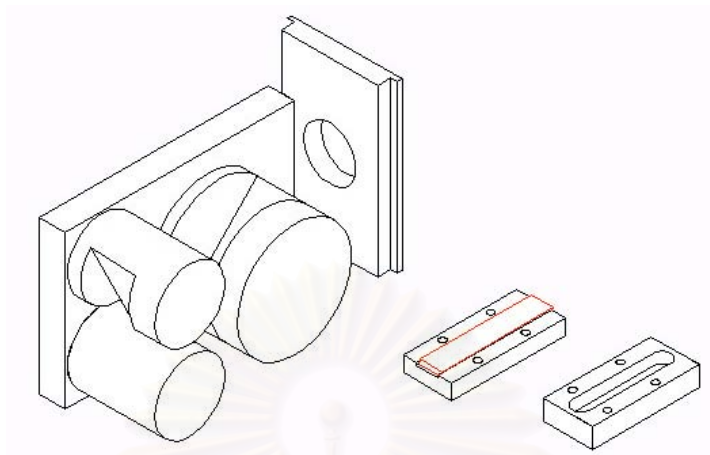


Figure 3.1 Illustration of new constructed accessory.

Infrared beam path going through the accessory is shown in figure 2. The infrared radiation from source enter the IRE at one end, reflects within the IRE and exit at the other end of IRE. The infrared radiation reflects at mirror M1 and mirror M2 before going to detector.

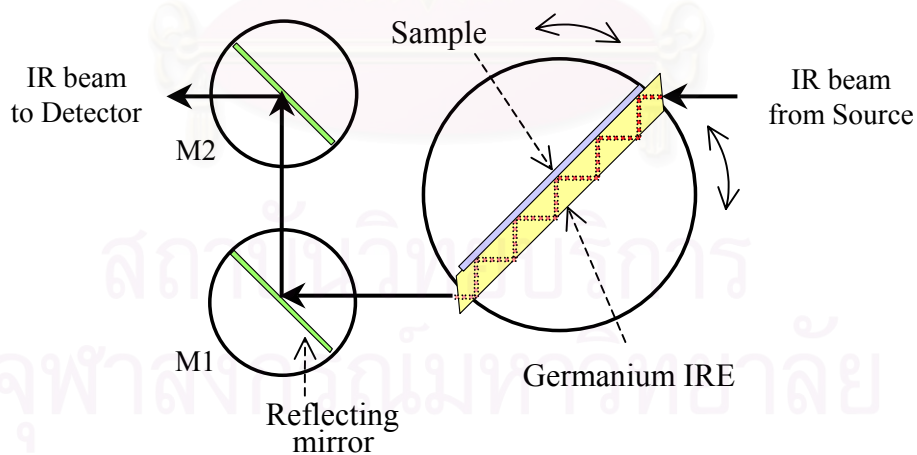


Figure 3.2 The optical diagram of the constructed accessory

3.2 Accessory Testing

3.2.1 Energy Throughput

3.2.1.1 Materials and equipment

Multiple attenuated total reflection (MATR) accessories

1. Baseline Multiple Reflection ATR accessory, 45° germanium IRE 50x5x2 mm (Spectra-Tech., Inc., Shelton, Connecticut, USA)
2. The Seagull™ accessory, hemisphere Germanium IRE 25 mm diameter (Harrick Scientific Corporation, Ossining, New York, USA)
3. Single-pass parallelepiped germanium plate IRE 30°, 45° and 60° (50x10x2 mm)

3.2.1.2 Testing Conditions

Spectrometer	Bruker Vector 33 FT-IR Spectrometer
Resolution	4.0 cm ⁻¹
Number of Scans	16
Result Spectrum	Absorbance
Source Setting	Globar (MIR)
Detector Setting	DTGS
Beam Splitter Setting	KBr

3.2.2.3 Energy Throughput Measurement

1. Energy throughputs of the Seagull™ and Baseline HATR accessories were recorded.
2. The constructed ATR accessory equips with 45° Germanium IRE was placed to FT-IR sample chamber.
3. The angle of incidence of accessory was adjusted to 45-degree by turning the knob of sample holder.
4. The reflecting mirrors were adjusted to optimum energy throughput by rotating and fine-tune the three screws behind mirrors.

5. Energy throughput was recorded.

6. Energy throughput of 30° and 60° angle of incidence germanium IRE were recorded by the same procedure as described in 2, 3, 4 and 5.

3.2.2 Chemical Testing

3.2.2.1 Materials and equipments

1. Multiple attenuated total reflection (MATR) accessories

1.1 Baseline Multiple Reflection ATR accessory, 45° germanium IRE 50x5x2 mm (Spectra-Tech., Inc., Shelton, Connecticut, USA)

1.2 The Seagull™ accessory, hemisphere Germanium IRE 25 mm diameter (Harrick Scientific Corporation, Ossining, New York, USA)

1.3 Single-pass parallelepiped germanium plate IRE 30°, 45° and 60° (50x10x2 mm)

2. Nujol

3.2.2.2 Testing Condition

Spectrometer	Bruker Vector 33 FT-IR Spectrometer
Resolution	4.0 cm ⁻¹
Number of Scans	16
Result Spectrum	Absorbance
Source Setting	Globar (MIR)
Detector Setting	DTGS
Beam Splitter Setting	KBr

3.2.2.3 Spectral Acquisitions

3.2.2.3.1. Polarize radiation

1. The constructed accessory equipped with 45° angle of incidence germanium IRE was aligned to the optimal condition (i.e., maximum energy throughput).
2. Background spectrum of 0 and 90 degree polarize light were collected.
3. Nujol was spreaded as a liquid film over germanium IRE and its ATR spectra were acquired.
4. Spectra of nujol using 30° and 60° angle of incidence germanium IRE were acquired by the same procedure described in 1, 2 and 3.
5. Spectra of nujol using the Seagull™ and Baseline HATR were acquired by the same procedure described in 1, 2 and 3.

3.2.2.3.2. Nonpolarize radiation

1. The constructed accessory equipped with 45° angle of incidence germanium IRE was aligned to the optimal condition (i.e., maximum energy throughput).
2. Background spectrum was collected.
3. Nujol was spreaded as a liquid film over germanium IRE and its ATR spectra were acquired.
4. Spectra of nujol using 30° and 60° angle of incidence germanium IRE were acquired by the same procedure described in 1, 2 and 3.
5. Spectra of nujol using the Seagull™ and Baseline HATR were acquired by the same procedure described in 1, 2 and 3.

3.2.3 Flowing of liquid

1. Water was utilized as flowing sample.
2. The inlet pipe of the constructed accessory was dipped in water and the outlet pipe was connected with pump.
3. ATR spectra of flowing water were acquired.

3.2.4 Spectral Simulation

In order to correct the angle of incidence of constructed accessory spectral simulation was programmed to compare experimental result with theory. Two-phase system was programmed using MATLAB (Appendix B and C). All equations in this program refer from Hansen equation [4].



สถาบันวิทยบริการ
จุฬาลงกรณ์มหาวิทยาลัย

CHAPTER 4

RESULTS AND DISCUSSION

4.1 Design and construction of accessory

The constructed accessory is shown in figure 4.1. The body of the accessory is made of high-grade aluminium. Therefore, the accessory is durable, low-cost, low weight, and simple to construct. The new accessory is designed by consider to the flowing of liquid sample without using pump, ease of alignment, and simplicity in operation. The accessory can be used with the existing commercially available spectrometer. The single-pass parallelepiped (SPP) germanium plate (50×10×2 mm) was employed as internal reflection element (IRE). The IRE was coupled with an aluminium plate. The flat aluminium plate stays in direct contact to lower side of the IRE. The upper side of the IRE contact with an o-ring. The IRE can be aligned with inclined angle (30, 45 and 60 degree) for free flow of liquid without an aid of a pump. Therefore, this new accessory can be utilized with flowing liquid and can be adapted for liquid, solid and powder sample.

The infrared beam direct into the IRE to the surface supporting the sample, and then redirect the internally reflected attenuated beam back into the detector by reflecting mirrors. In order to enhance the energy throughput, the Ni-Co-Al alloy reflecting mirror was coated with gold by sputtering. It is then employed as the reflecting mirrors. The Ni-Co-Al alloy from the computer hard drive is cheaper than commercial reflecting mirrors but gives the comparable energy throughput. The reflecting mirror can be fine-tune in order to adjust to enhance energy throughput.

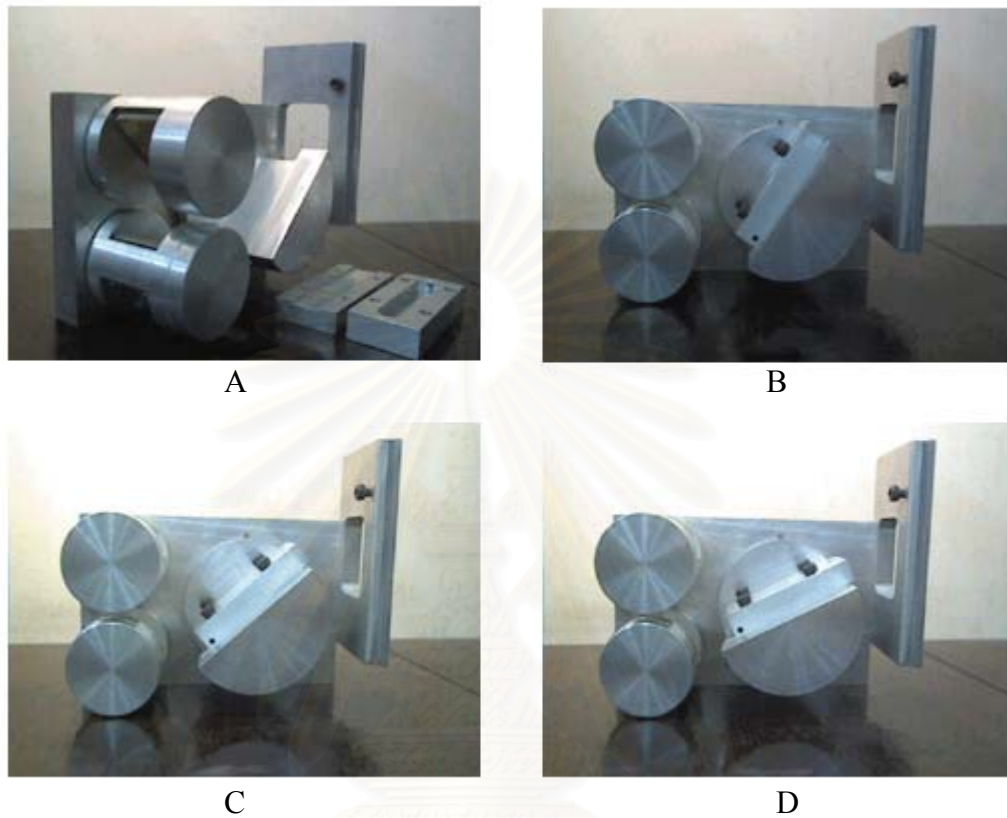


Figure 4.1 (A) the constructed accessory. (B) the constructed accessory equipped with 30° angle of incidence (C) the constructed accessory equipped with 45° angle of incidence (D) the constructed accessory equipped with 60° angle of incidence

สถาบันวิทยบริการ
จุฬาลงกรณ์มหาวิทยาลัย



Figure 4.2 Photograph of the Baseline HATR equipped with Single-pass trapezoidal germanium plate



Figure 4.3 Photograph of the Seagull™

4.2 Testing of the accessory

4.2.1 Energy Throughput

The constructed accessory was tested with Fourier Transform Infrared (FT-IR) Spectrometer. The Ni-Co-Al alloy was used as reflecting mirrors. At first, it isn't coated with gold. The energy throughput of accessory equipped with 45° single-pass parallelepiped (SPP) germanium plate was compared with commercially accessory, Baseline HATR equipped 45° single-pass trapezoidal (SPT) germanium plate. The interferogram and single beam spectra of the constructed accessory and Baseline HATR are shown in Figure 4.4 and 4.5, respectively. Due to their physical dimension and angle of incidence are the same, thus the energy throughputs are also possibly the same. An optimum alignment the energy throughput obtained from the constructed accessory is lower than that obtained from Baseline HATR. Their energy throughputs are 3348 and 9460 for the constructed and Baseline HATR accessories, respectively. The interferogram signal and the single beam spectra response acquired via the Baseline HATR are higher in intensity than that obtained from the constructed accessory. These are due to the low energy reflected by Ni-Co-Al alloy, which is utilized as reflecting mirror.

In order to enhance the energy throughput, the reflecting mirror was coated with gold. The energy throughput, interferogram and single beam spectra obtained from the accessory after coating with gold are shown in Figure 4.6. The energy throughput increases when the gold-coated reflecting mirror is employed. The energy throughput is 10180, which is higher than that obtained from the noncoated reflecting mirror. It is also higher than that using the Baseline HATR accessory. The interferogram signal and single beam spectra response acquired via accessory are higher than that without gold-coated reflecting mirror. The high-energy throughput is due to the good reflected mirror and fine-adjustable reflecting mirror.

The interferogram and single beam spectra acquired via the Seagull™ equipped with germanium hemisphere are shown in Figure. 4.7. Due to the number

of reflections of the Seagull™ is only 1.0, and the infrared beam can travel through the hemisphere shape IRE with large area. The energy throughput obtained from the Seagull™ is greater than that obtained from the constructed and the Baseline HATR accessories due to much less loss in energy. The energy throughput from the Seagull™ is 20578.



สถาบันวิทยบริการ
จุฬาลงกรณ์มหาวิทยาลัย

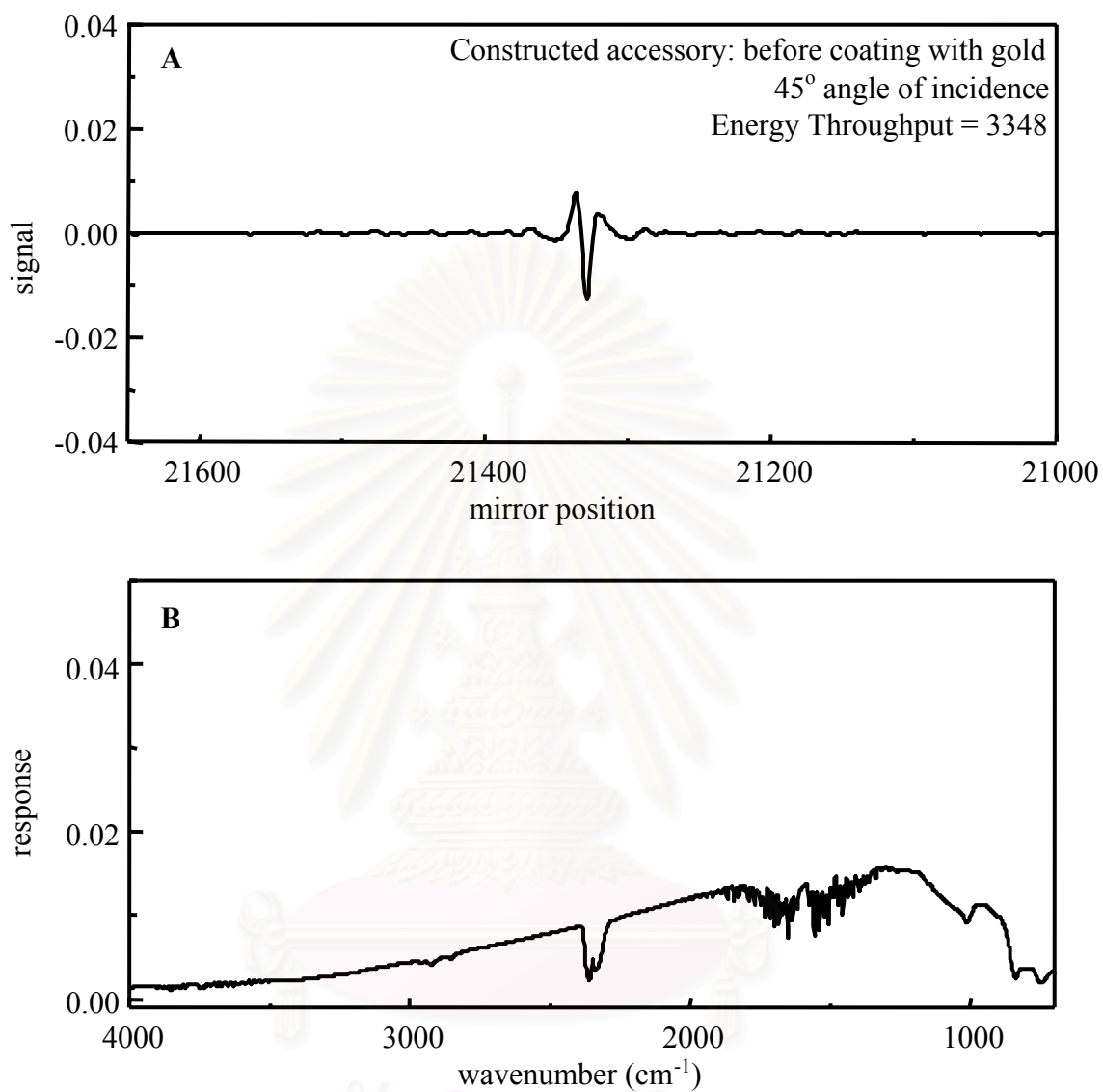


Figure 4.4 (A) Interferogram and (B) single beam spectra of air acquired via the 45° constructed accessory before the reflecting mirror is coated with gold.

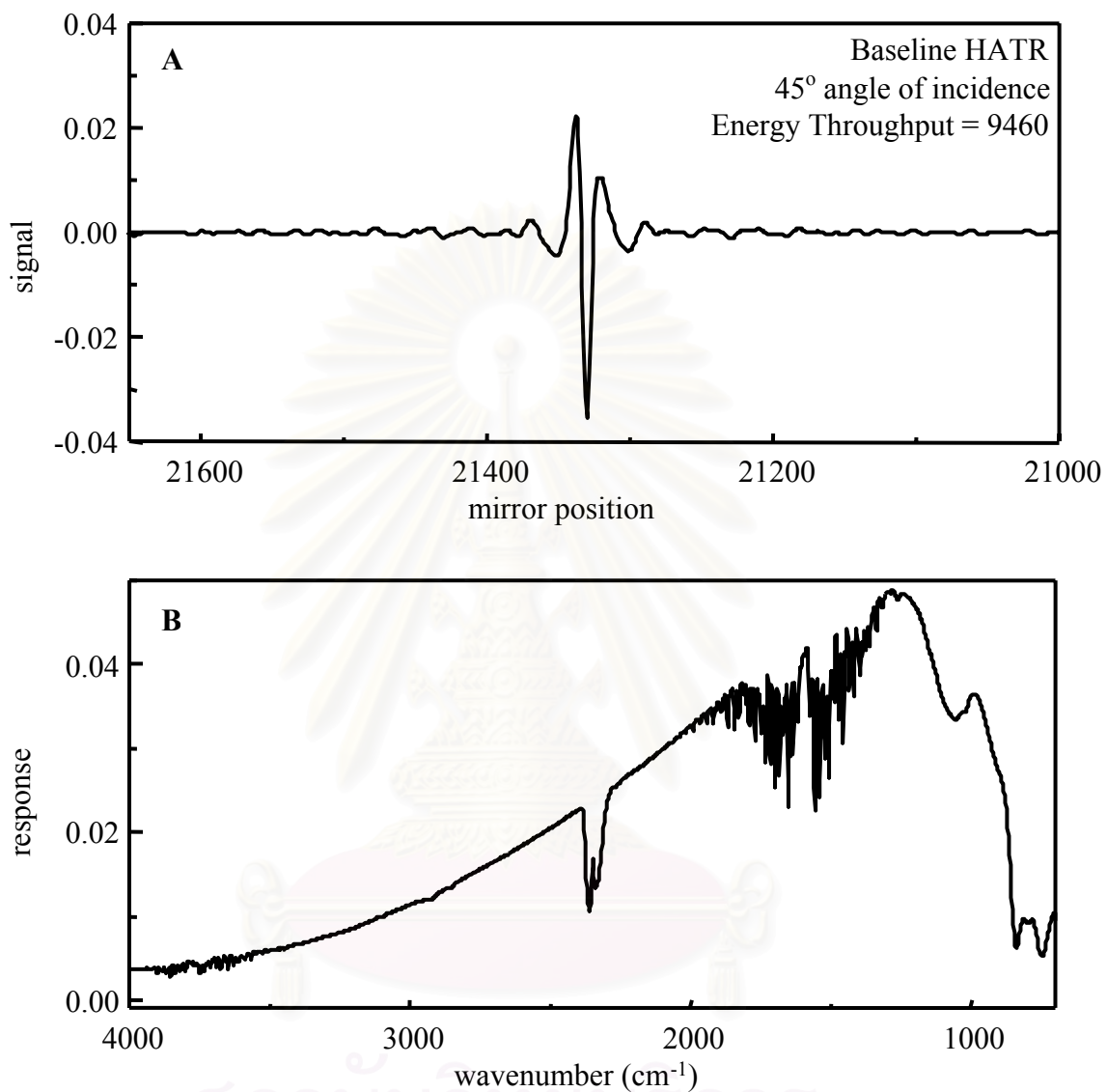


Figure 4.5 (A) Interferogram and (B) single beam spectra of air acquired via Baseline HATR accessory.

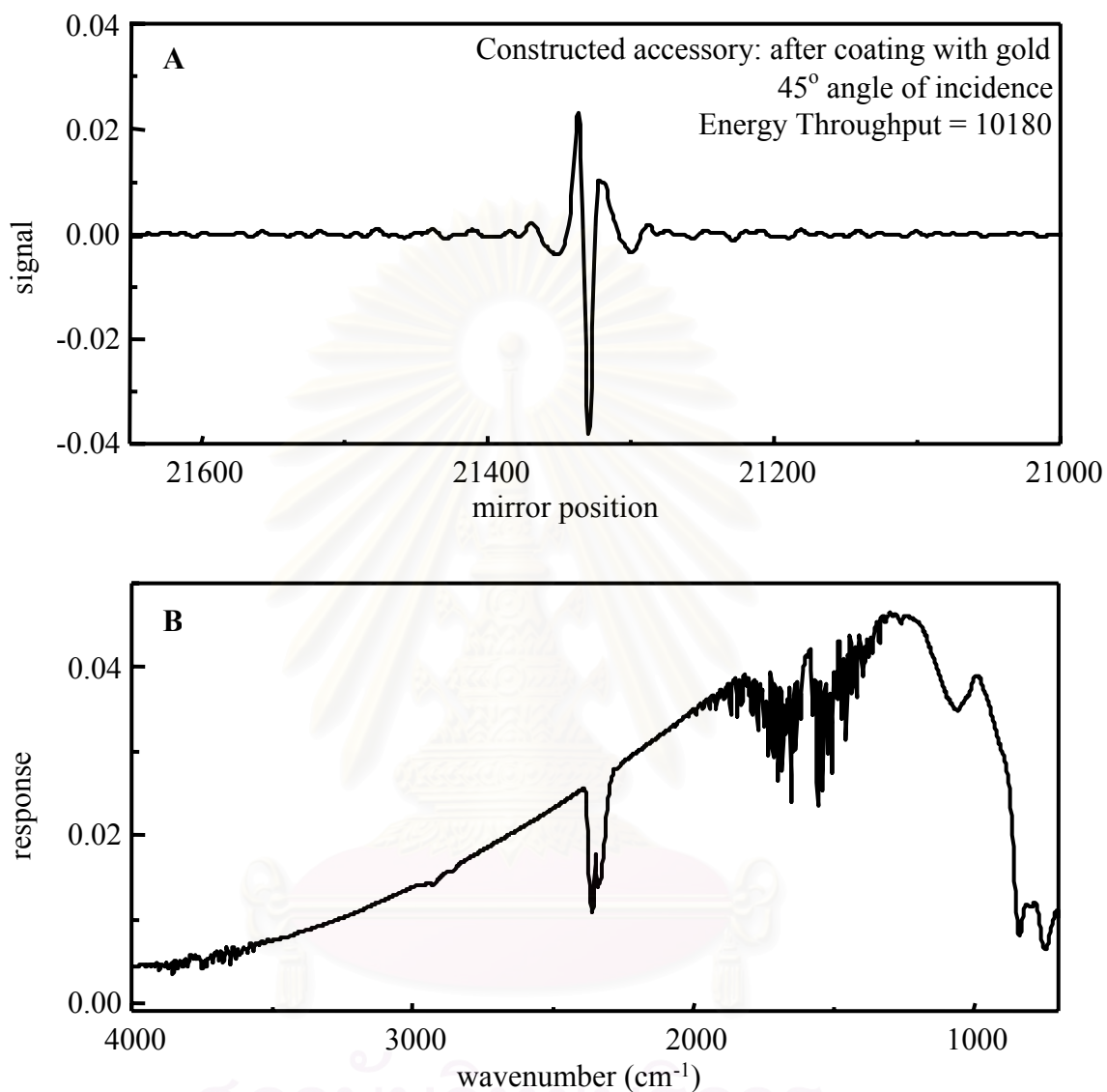


Figure 4.6 (A) Interferogram and (B) single beam spectra of air acquired via the 45° constructed accessory after the reflecting mirror is coated with gold.

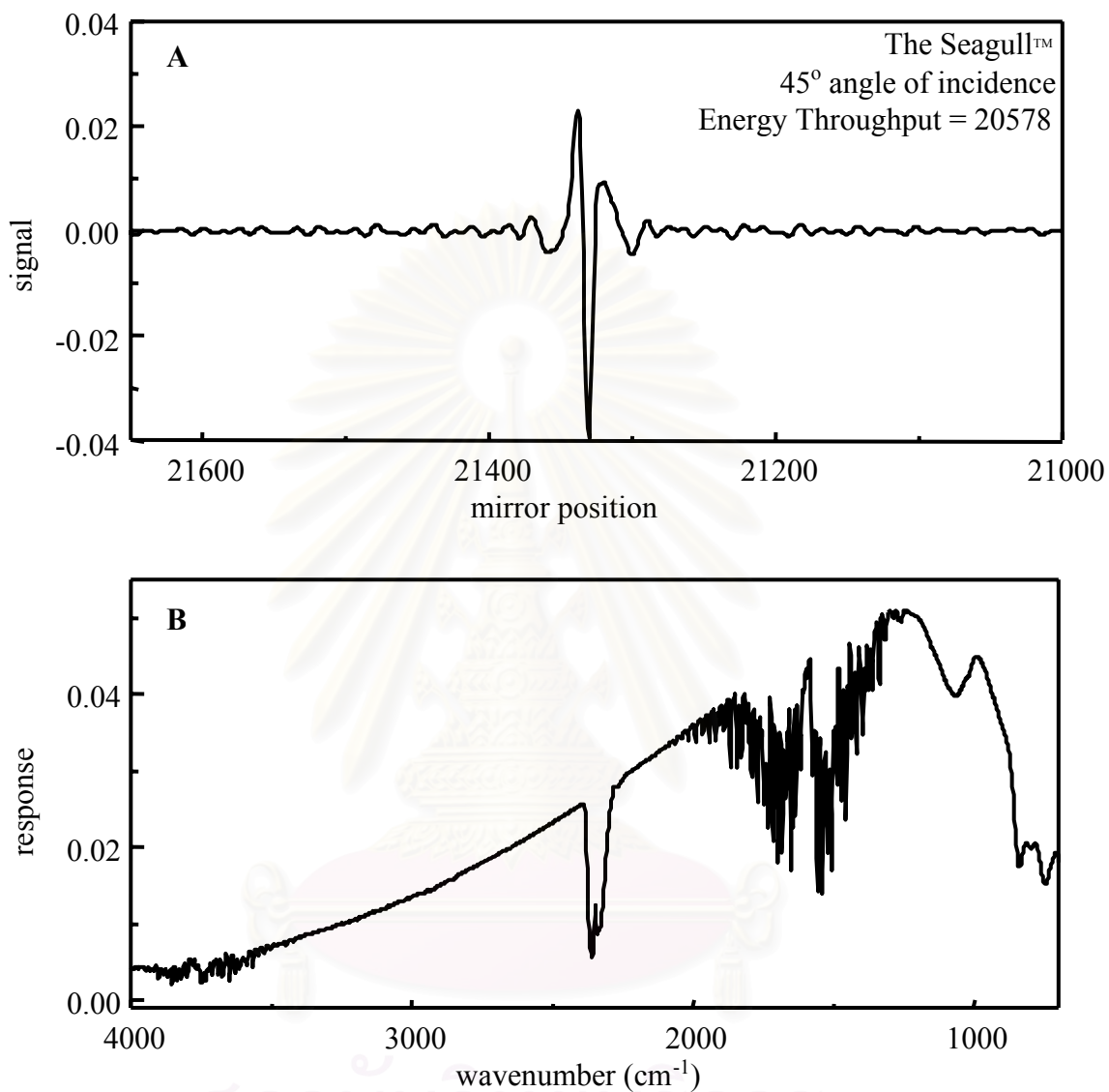


Figure 4.7 (A) Interferogram and (B) single beam spectra of air acquired via the 45° Seagull™ accessory.

In order to compare the performance between noncoated and gold-coated reflecting mirrors of constructed accessory, their energy throughputs of each angle are compared and shown in Figures 4.8-4.13. The energy throughputs obtained from the accessory equipped with the gold-coated reflecting mirror are significantly greater than that obtained from that with original reflecting mirror. At 30° angle of incidence, the energy throughput of before and after gold-coated reflecting mirror accessory are 2314 and 5207, respectively. At 45° angle of incidence, the energy throughput of before and after gold coated reflecting mirror accessory are 3348 and 10180, respectively. At 60° angle of incidence, the energy throughput of before and after gold-coated reflecting mirror accessory are 2642 and 5369, respectively. From the results, the energy throughputs of the gold-coated reflecting mirrors are greater than those with noncoated reflecting mirror due to reflecting efficiency of the gold-coated mirror.

Compared between different angle of incidence (30°, 45° and 60°), the energy throughput obtained from 45° angle of incidence is greater than that obtained from 60° and 30°, respectively. The energy throughput depends on aperture, number of reflections and angle of incidence on the IRE. Their theoretical apertures are 2.83, 2.31 and 2.00 for 45°, 60° and 30° angle of incidence IRE, respectively. The 30° angle of incidence IRE has highest number of reflections, number of reflections is 43.6, and small entrance aperture. Therefore the energy throughput obtained from 30° angle of incidence is lower than those obtained from 45° and 60°. The high energy throughput of 45° angle of incidence IRE is due to the biggest aperture. The infrared beam can enter the aperture to 45° angle of incidence IRE more than other IRE. Although, the 60° angle of incidence has lower number of reflections but the energy throughput is lower compared with the 45° angle of incidence IRE, because the divergent beam will tend to fill the entire plate as it transverses the length of the plate. Therefore some of the infrared beam will approach the exit aperture from the wrong direction and be totally reflected by this aperture and be lost even when the exit aperture is placed at the correct location for the central ray [2].

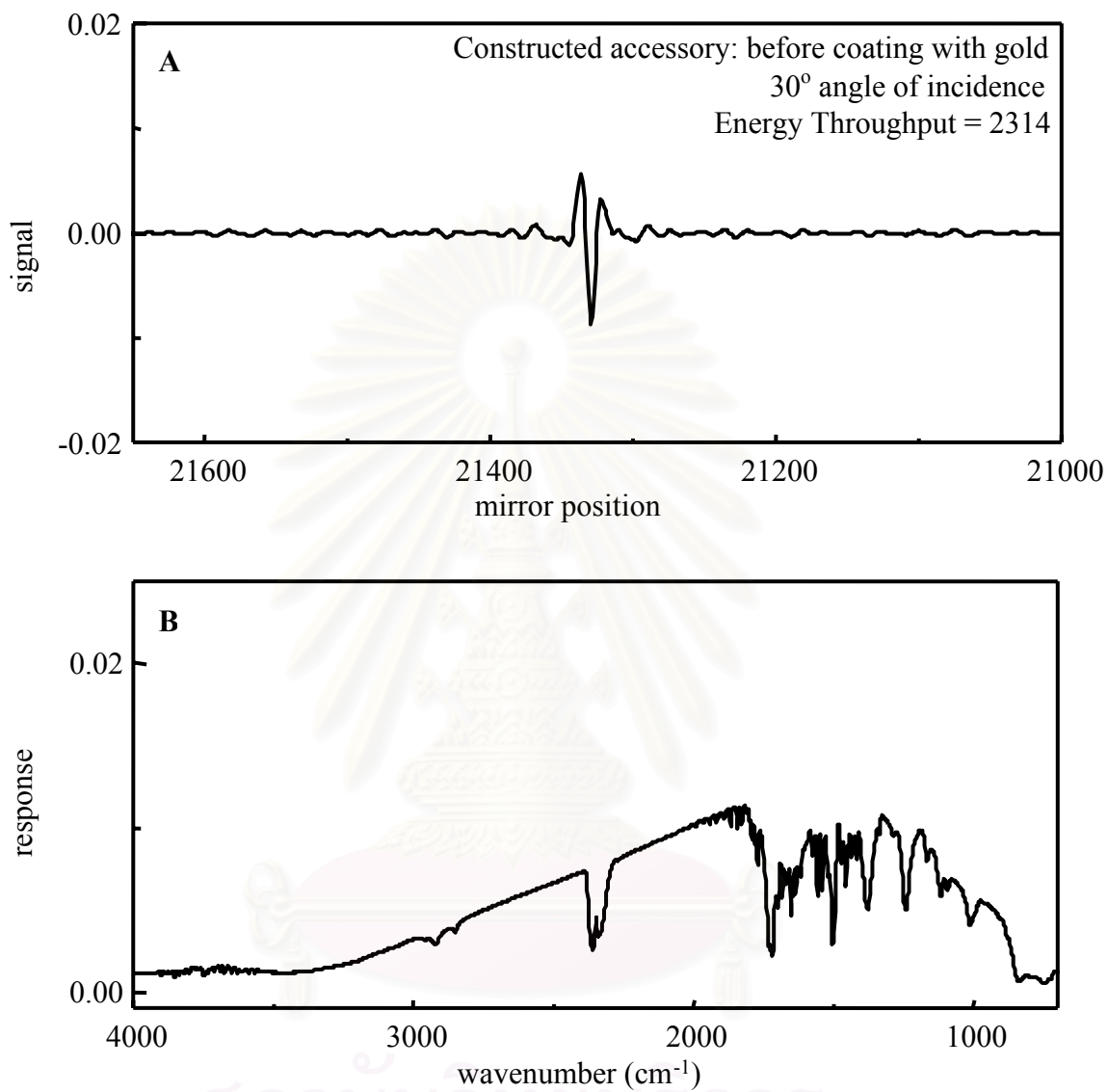


Figure 4.8 (A) Interferogram and (B) single beam spectra of air acquired via the 30° constructed accessory before the reflecting mirror is coated with gold.

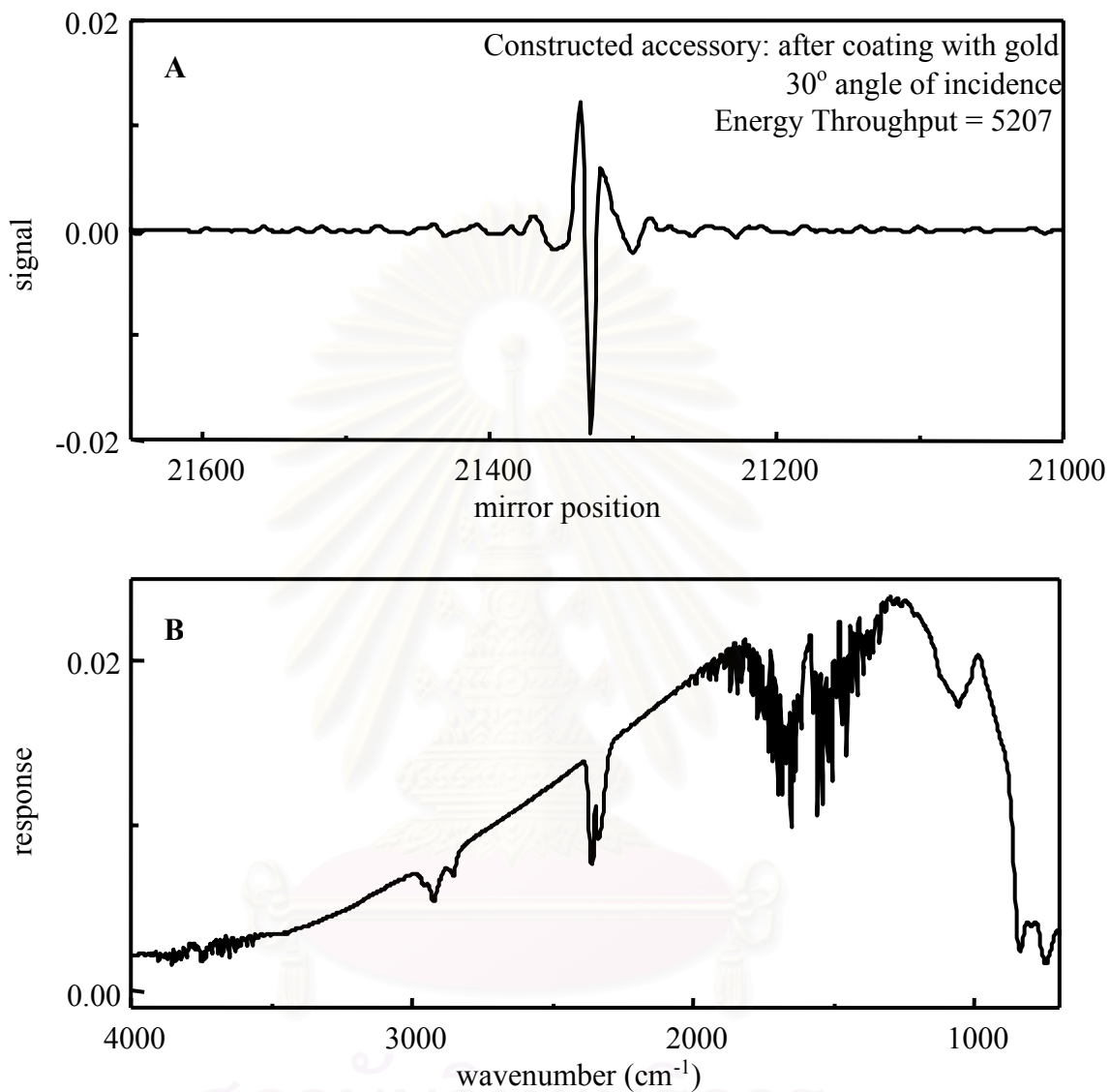


Figure 4.9 (A) Interferogram and (B) single beam spectra of air acquired via the 30° constructed accessory after the reflecting mirror is coated with gold.

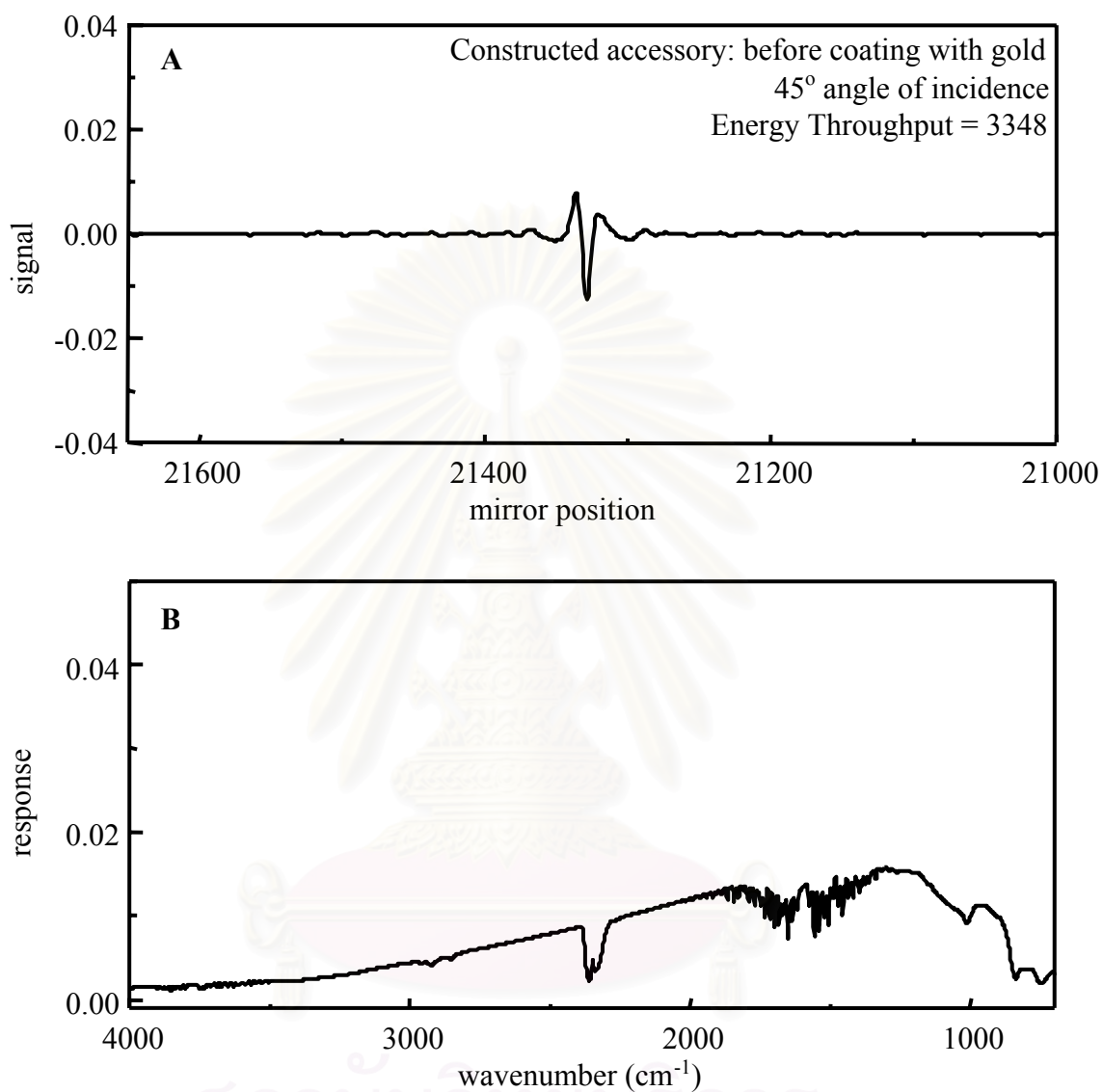


Figure 4.10 (A) Interferogram and (B) single beam spectra of air acquired via the 45° constructed accessory before the reflecting mirror is coated with gold.

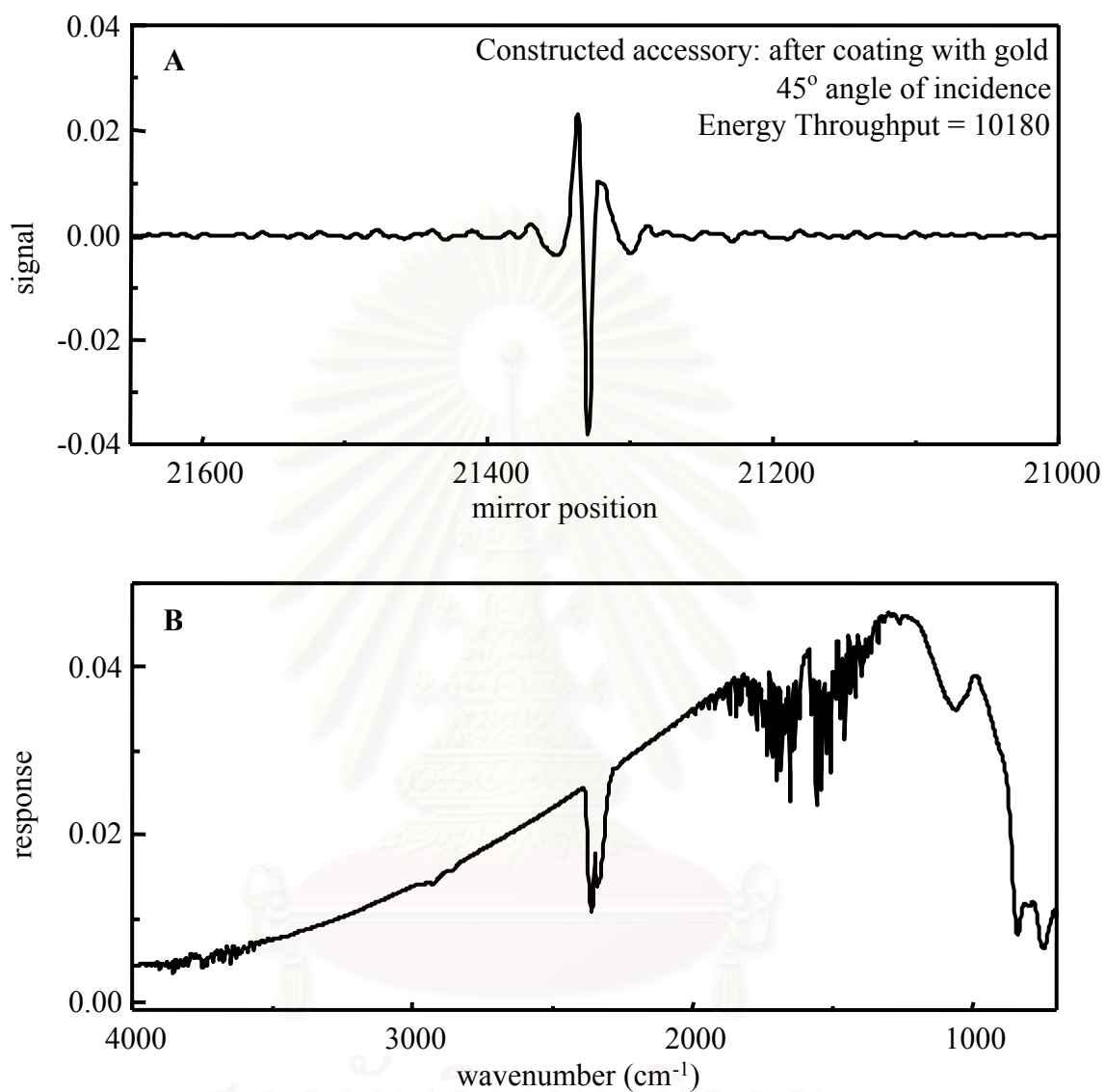


Figure 4.11 (A) Interferogram and (B) single beam spectra of air acquired via the 45° constructed accessory after the reflecting mirror is coated with gold.

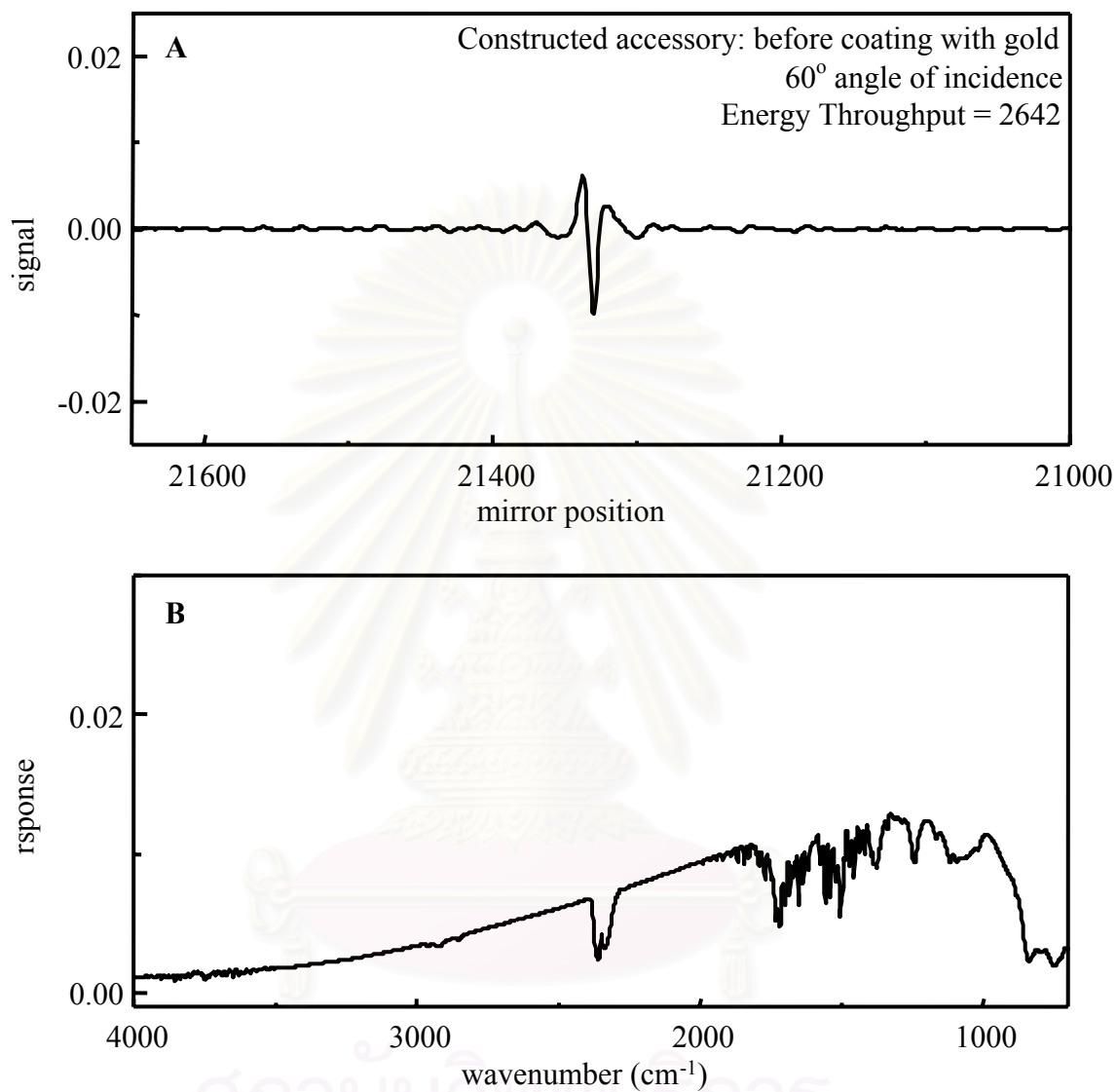


Figure 4.12 (A) Interferogram and (B) single beam spectra of air acquired via the 60° constructed accessory before the reflecting mirror is coated with gold.

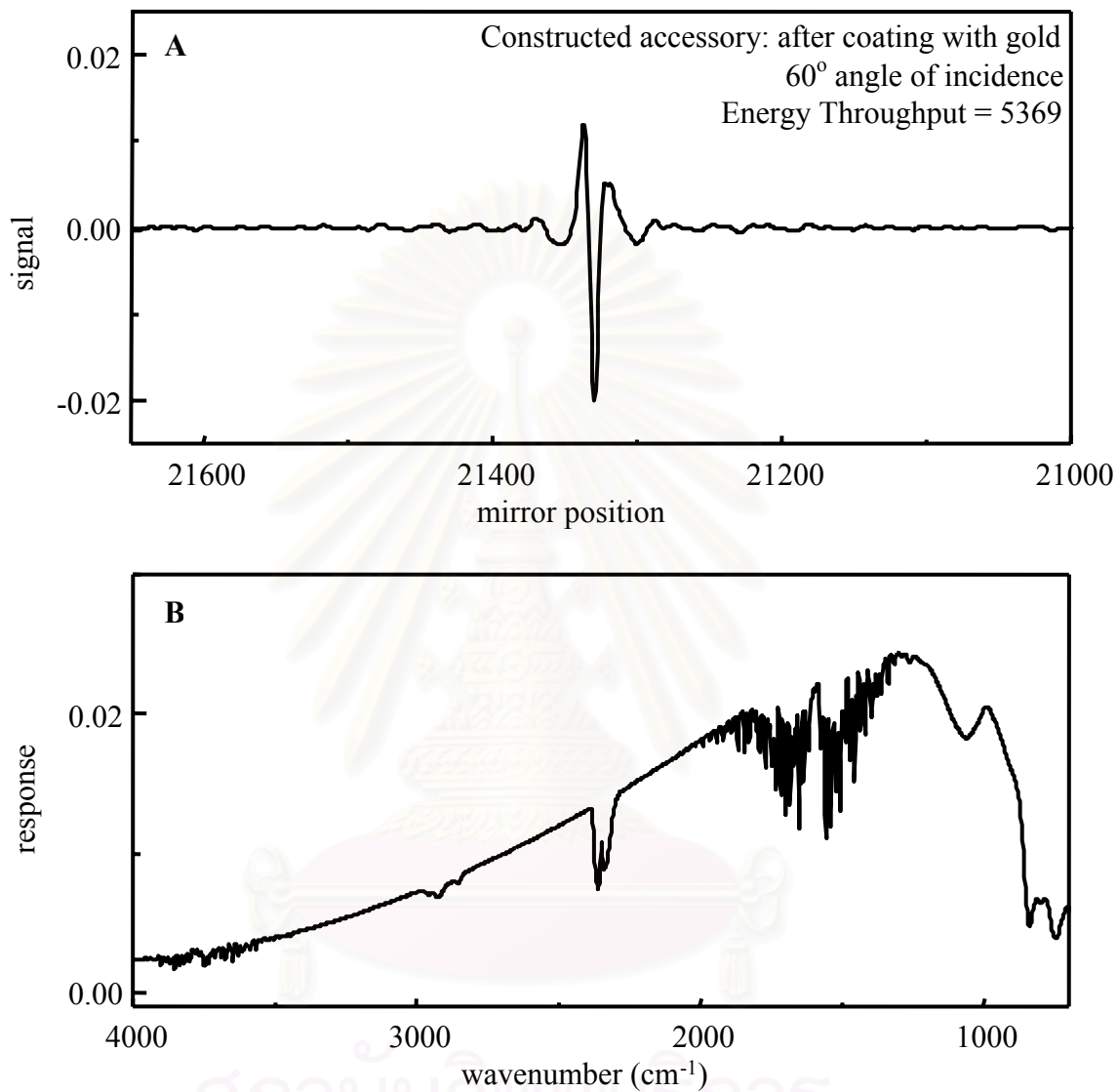


Figure 4.13 (A) Interferogram and (B) single beam spectra of air acquired via the 60° constructed accessory after the reflecting mirror is coated with gold.

4.2.2 Chemical Testing

A comparison between the result from the constructed accessory and that from a commercial accessory is shown in Figure 4.14. There are ATR spectra of nujol (non-polarized, s-polarized and p-polarized radiation) obtained from the Baseline HATR accessory, the Seagull™, and the constructed accessory at 45° angle of incidence IRE. In order to eliminate the problem related to corrosion and vaporization of chemical substance, a liquid sample: nujol, is utilized in this experiment. An acceptable spectral quality is obtained from the constructed accessory. The characteristic peaks of nujol obtained from the constructed accessory are exactly the same in position as that obtained from the Baseline HATR and the Seagull™ (i.e., peak position). Since the ATR spectral intensity is proportional to quantity of liquid sample as interact with infrared radiation. Therefore ATR spectra acquired via constructed accessory and the Baseline HATR accessory are higher than that acquired via the Seagull™ due to larger amount of nujol spreaded on IRE. In addition, the ATR spectra obtained from constructed accessory is higher than that obtained from the Baseline HATR due to the same reason. Because of the great energy throughput of the Seagull™ and the constructed accessory, their signal to noise (S/N) ratio is higher than S/N of the Baseline HATR. The base line of ATR spectra is smoother than that obtained from the Baseline HATR. In case of the Seagull™ its energy throughput and the signal to noise ratio is high. This is due to the new IRE and the low number of reflections of the Seagull™, i.e. the number of reflections is one.

ATR spectra of nujol collected by the constructed accessory, the Baseline HATR and the Seagull™ using s-polarized radiation (the dash line) non-polarized radiation (the solid line) and p-polarized radiation (the dot line) are shown in this figure. Theoretically, at 45° angle of incidence, the intensity of p-polarized radiation ATR spectrum is twice of that of s-polarize ATR spectrum. In case of the Baseline HATR and the Seagull™ accessories, the intensity of p-polarize ATR spectrum is two times higher that of s-polarize ATR spectrum. The new accessory has the same

results as the Baseline HATR accessory. Therefore, the angle of new accessory is correct.

ATR spectra of nujol collected by the constructed accessory, the Seagull™ using s-polarized radiation (the dash line), non-polarized radiation (the solid line), and p-polarized radiation (the dot line) at 30° and 60° angle of incidence are shown in figure 4.15 and 4.16, respectively. The peak positions of spectra from the constructed accessory are the same as that from the Seagull™. The spectra intensity of constructed accessory is higher than that the Seagull™ due to different amount of nujol as spreaded on IRE. The spectra intensity obtained from 30° angle of incidence are higher than that obtained from 60° angle of incidence. This observation agree very well with the theory.

ATR spectra of nujol collected by the constructed accessory at different angle of incidence (30°, 45° and 60°) are shown in Figure 4.17. Theoretically, the ATR spectra intensity collected via 30° angle of incidence IRE is higher than that collected via 45° and 60° angle of incidence IRE, respectively, due to the higher penetration depth than the others. The upper figure shows the ATR spectra of nujol at 30° angle of incidence. The peak positions of constructed accessory are the same as obtained from 45° and 60° angle of incidence but peak heights of 30° angle of incidence are higher than that of 45° and 60° angle of incidence. The observation agree very well with the theory.

สถาบันวิทยบริการ
จุฬาลงกรณ์มหาวิทยาลัย

Table 4.1 Dimensions and number of reflections of internal reflection element (IRE) in attenuated total reflection (ATR) accessories.

ATR Accessory	Dimension (l×w×t) mm	Number of reflections
The Baseline HATR	50×5×2	12.5
The Seagull™	Hemisphere Radius 12.5	1.0
30° Constructed flow cell	50.4×10×2	21.8
45° Constructed flow cell	50×10×2	12.5
60° Constructed flow cell	50.8×10×2	7.35

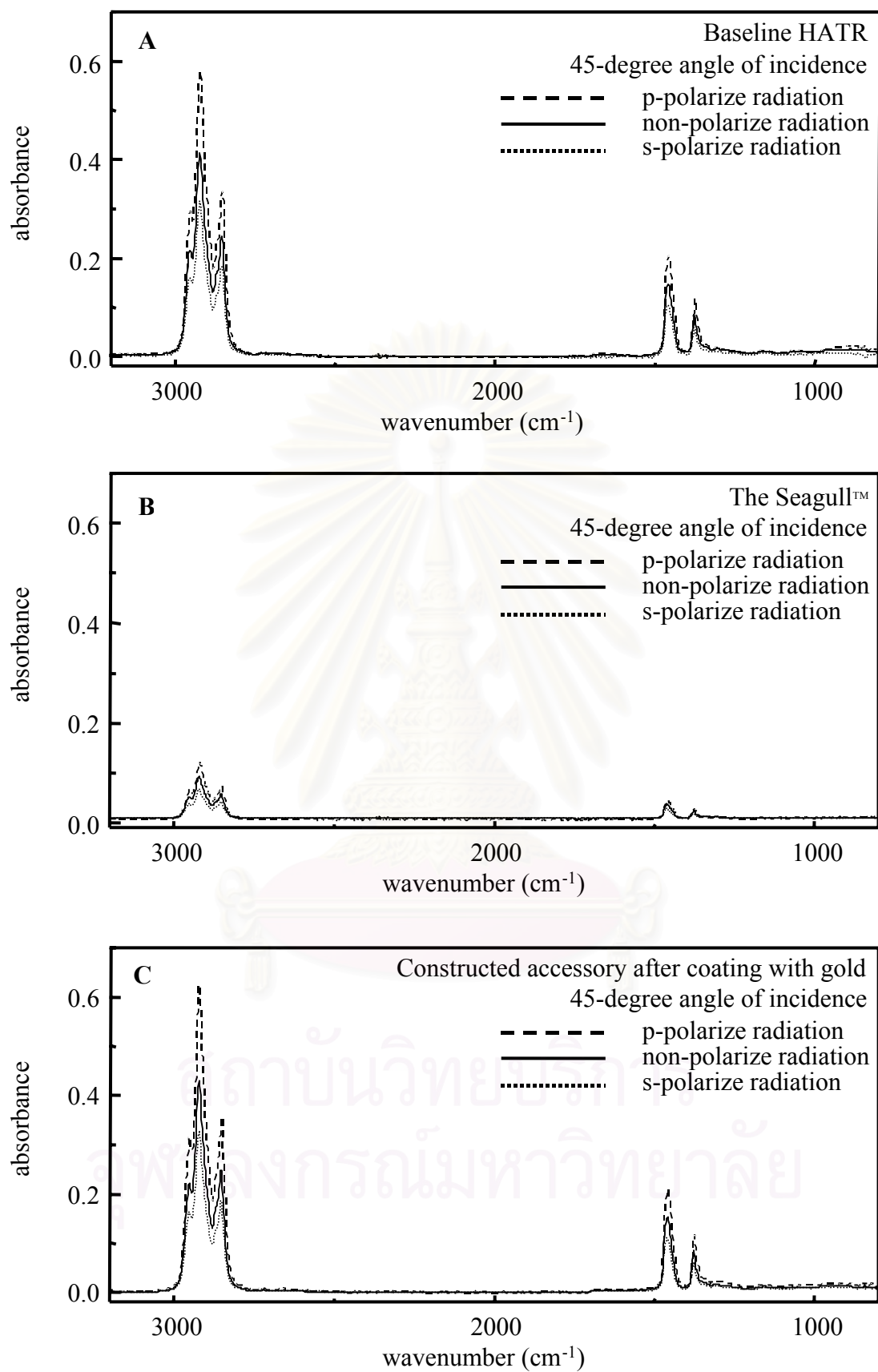


Figure 4.14 ATR spectra of nujol acquired via (A) The Baseline HATR (B) The Seagull™ (C) The constructed accessory after the reflecting mirror is coated with gold at 45° angle of incidence.

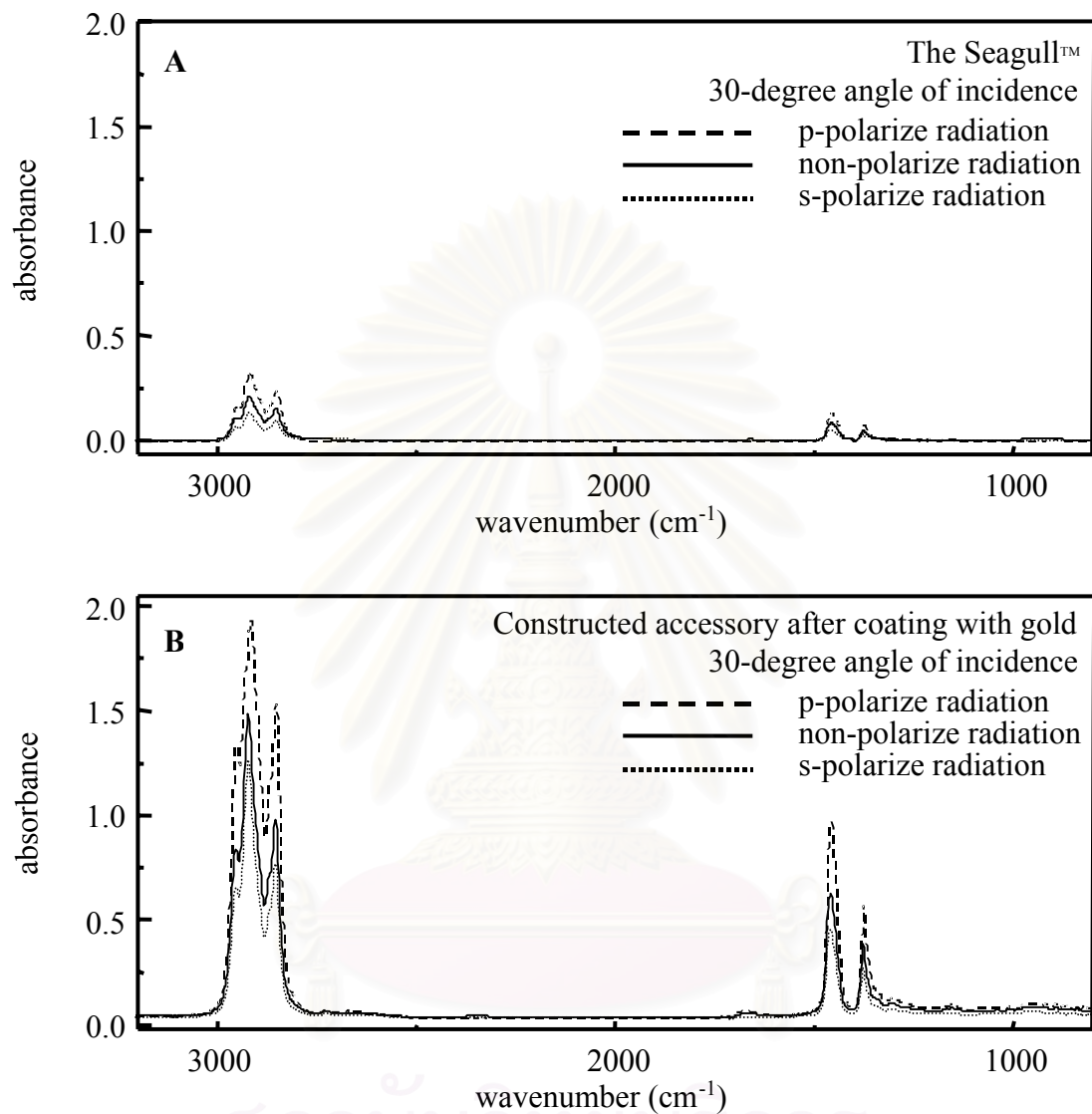


Figure 4.15 ATR spectra of nujol acquired via (A) The Seagull™ at 30° angle of incidence. (B) The constructed accessory after the reflecting mirror is coated with gold at 30° angle of incidence.

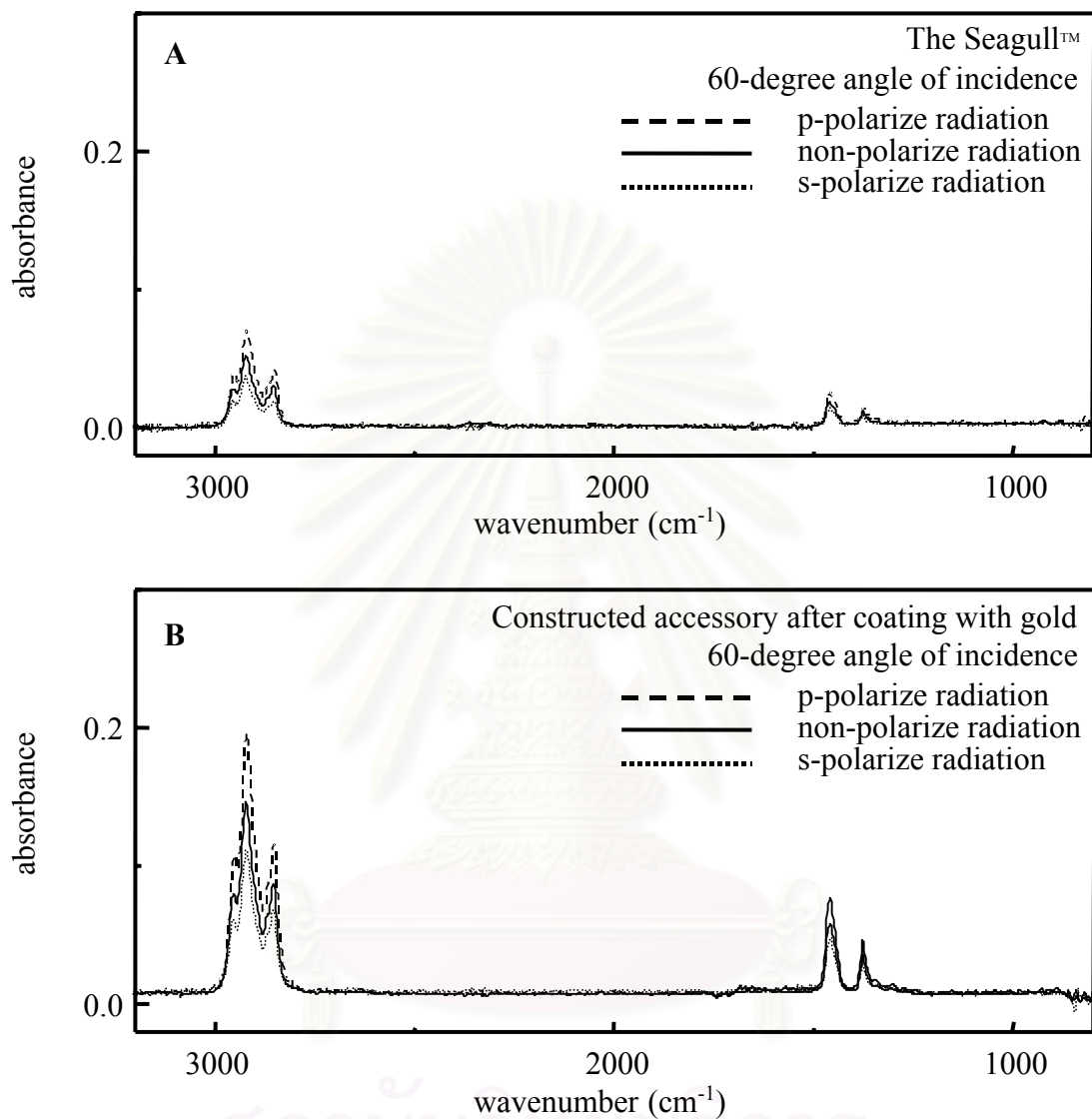


Figure 4.16 ATR spectra of nujol acquired via (A) The Seagull™ at 60° angle of incidence. (B) The constructed accessory after the reflecting mirror is coated with gold at 60° angle of incidence.

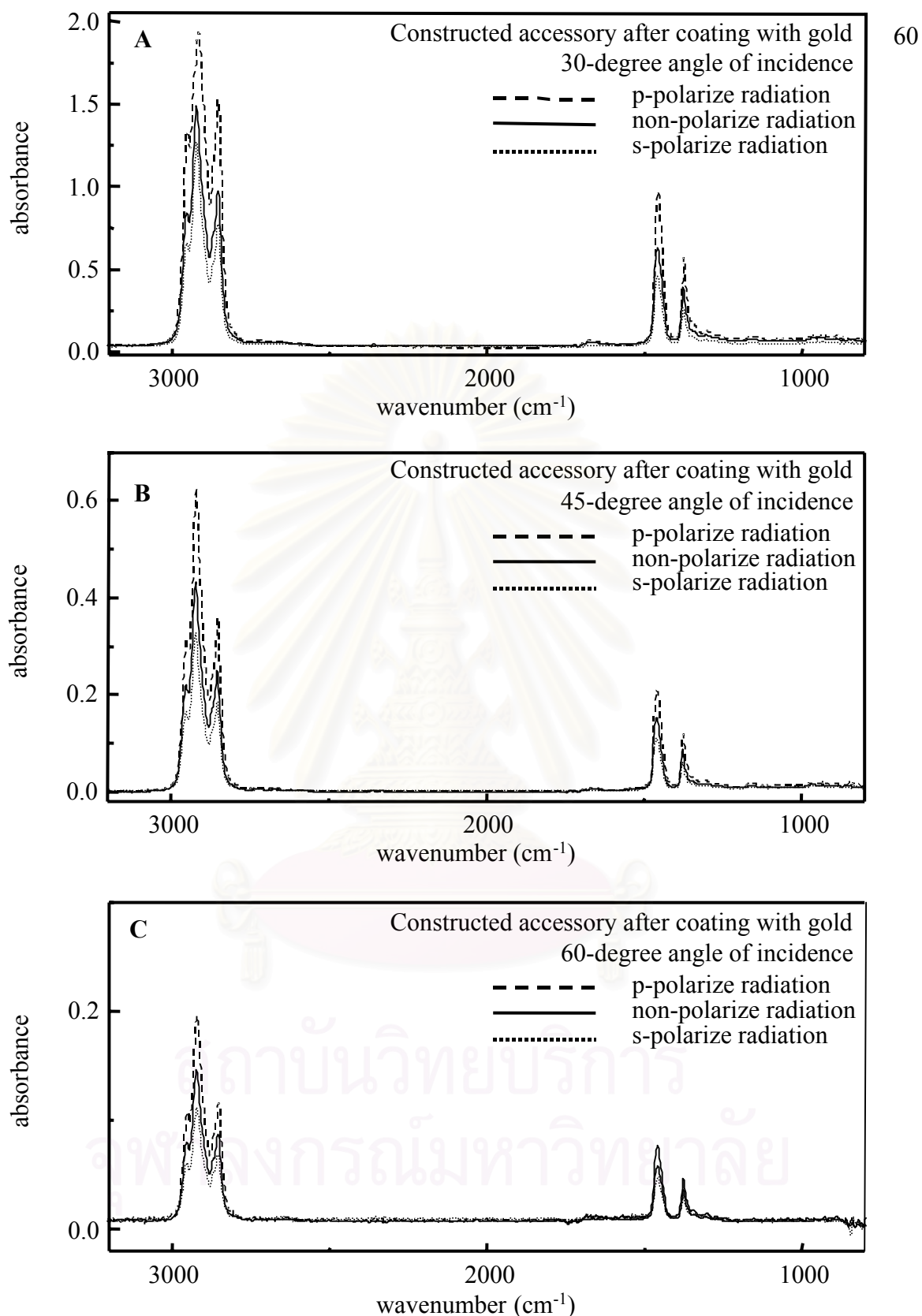


Figure 4.17 ATR spectra of nujol acquired via the constructed accessory after the mirror was coated with gold equip with (A) 30° angle of incidence (B) 45° angle of incidence (C) 60° angle of incidence.

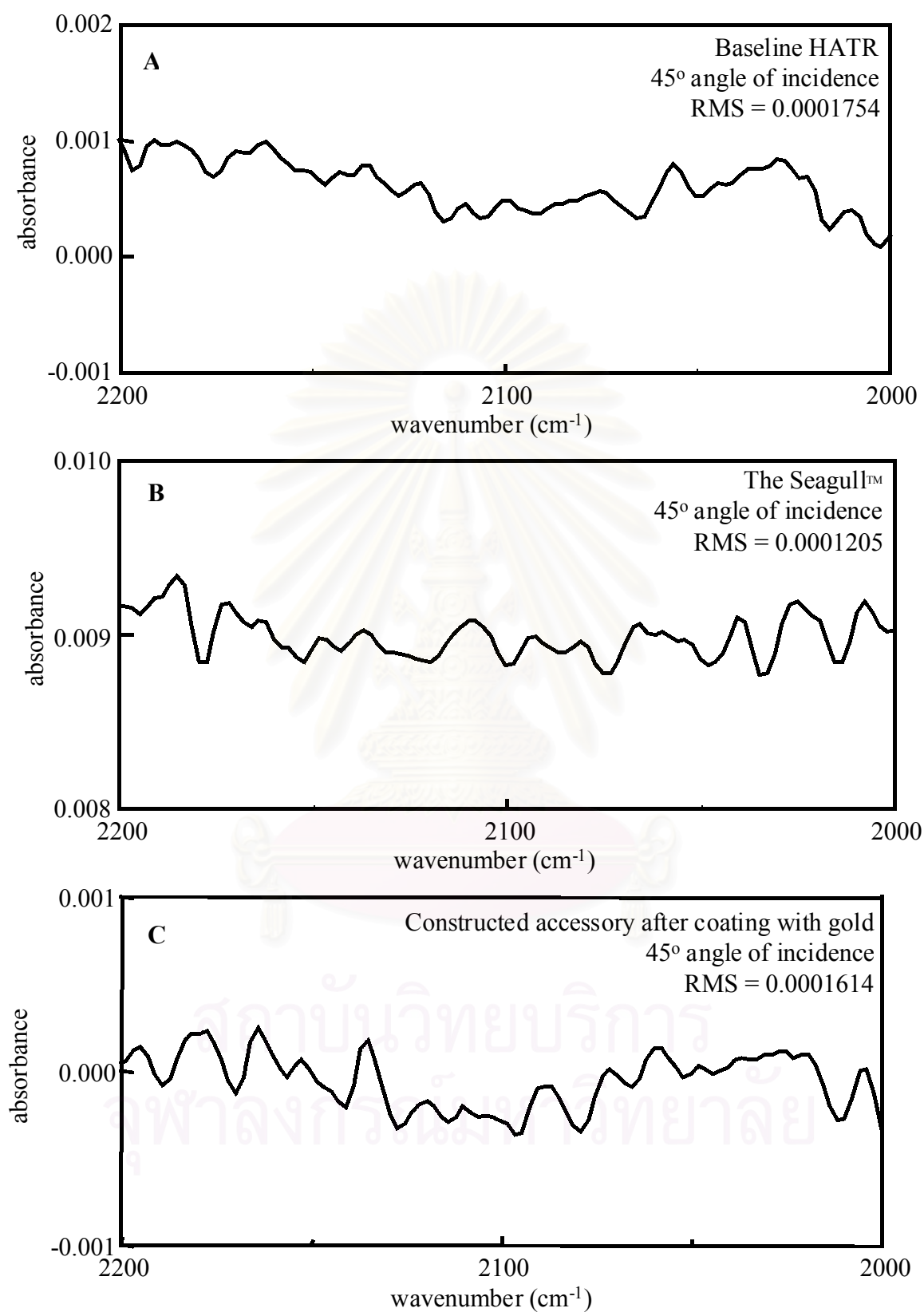


Figure 4.18 ATR spectra of nujol between 2200-2000 cm^{-1} at 45° angle of incidence (A) Baseline HATR (B) Seagull™ and (C) constructed accessories.

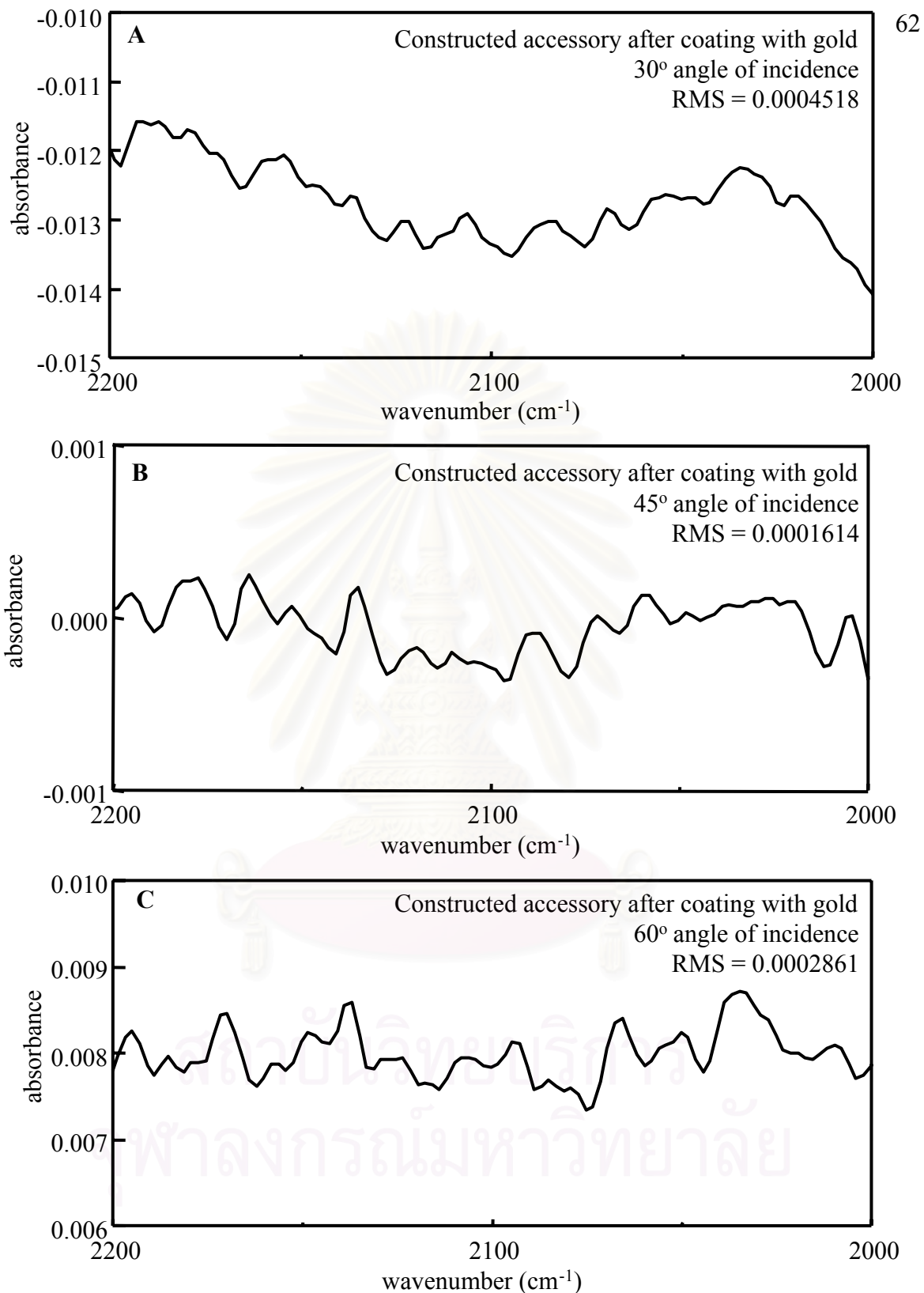


Figure 4.19 ATR spectra of nujol of the constructed accessory between 2200-2000 cm⁻¹ (A) 30° (B) 45° (C) 60°

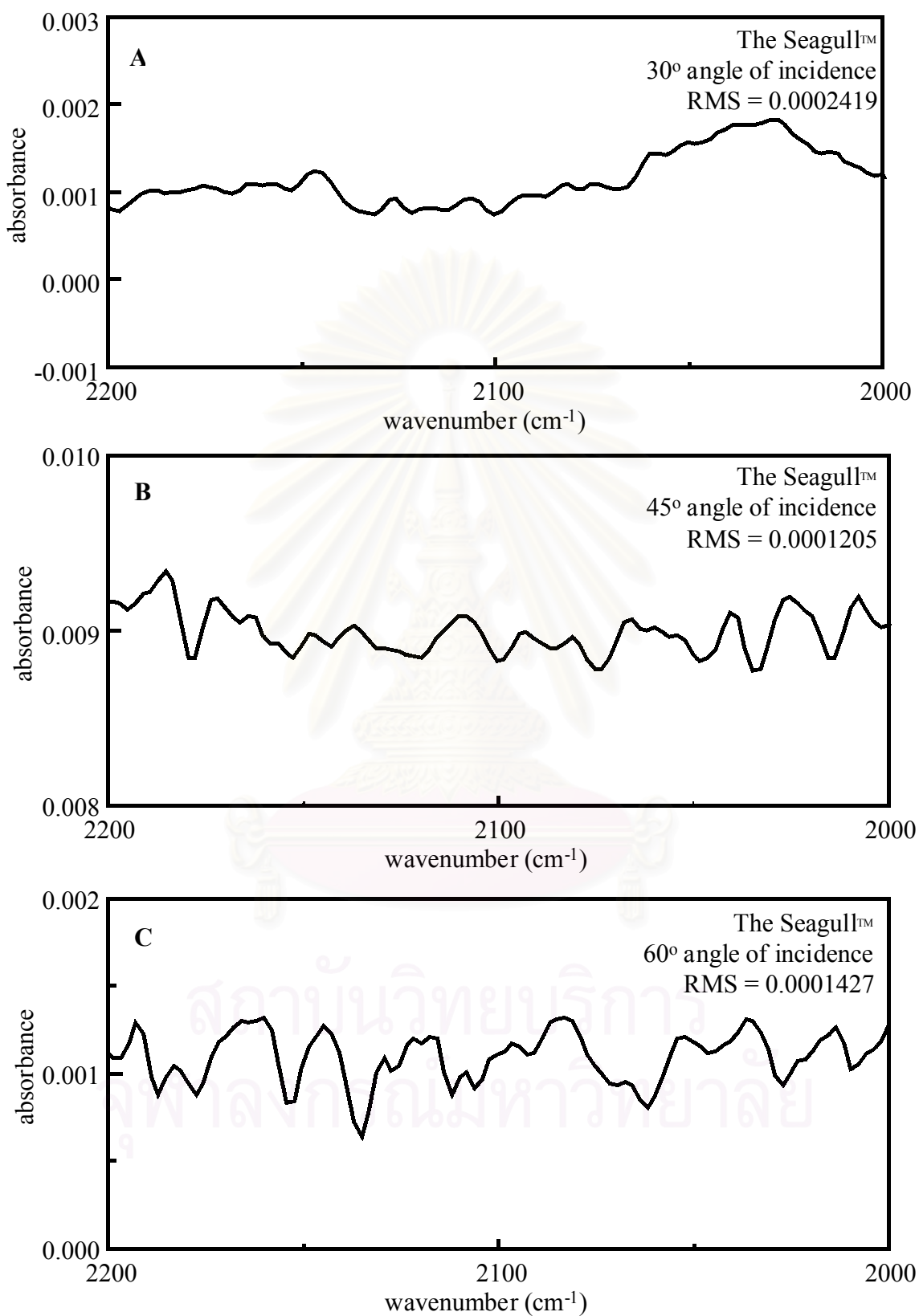


Figure 4.20 ATR spectra of nujol of the Seagull™ between 2200-2000 cm⁻¹ (A) 30° (B) 45° (C) 60°

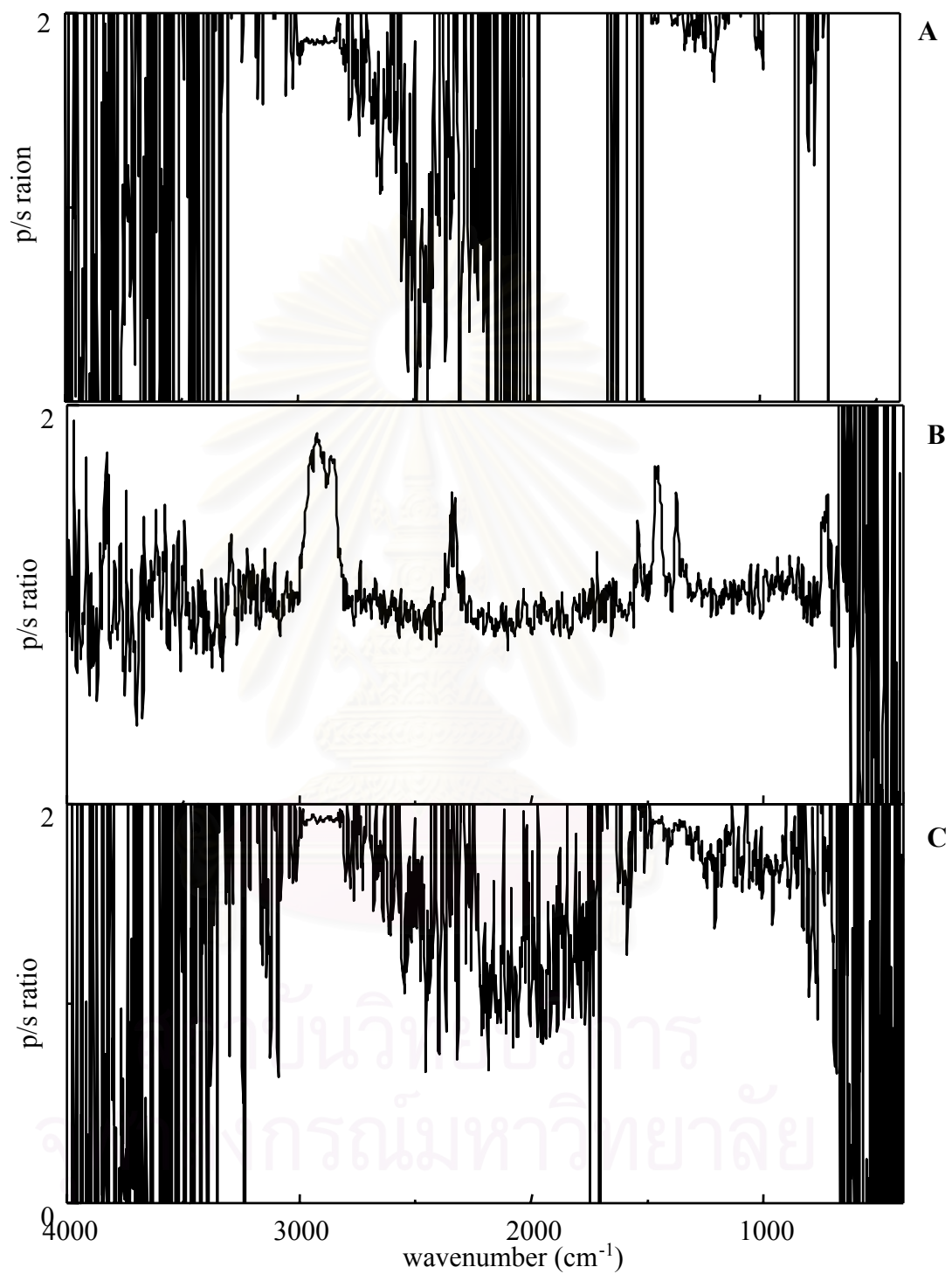


Figure 4.21 p/s ratio (A) Baseline HATR (B) constructed accessory 45° angle of incidence (C) Seagull 45° angle of incidence

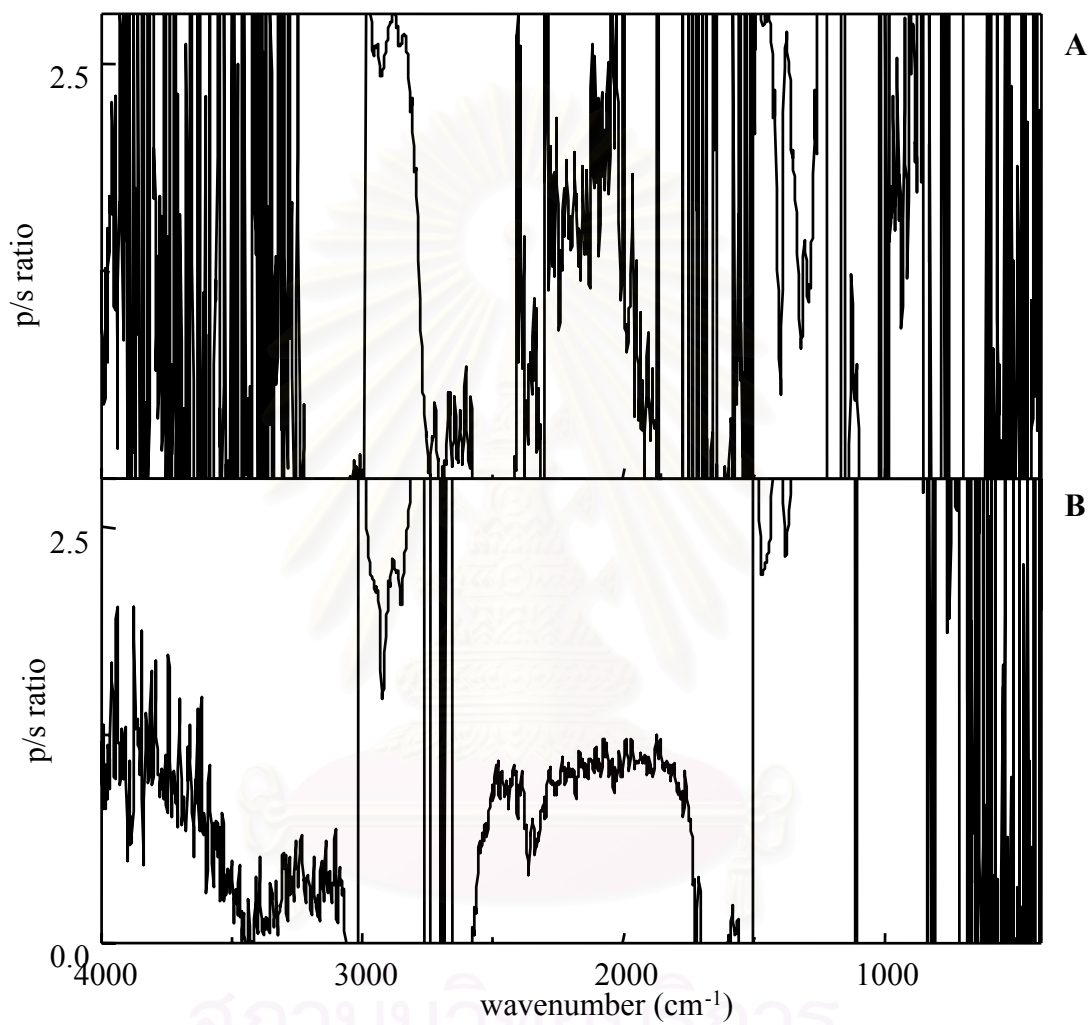


Figure 4.22 p/s ratio (A) Seagull 30° angle of incidence (B) constructed accessory 30° angle of incidence

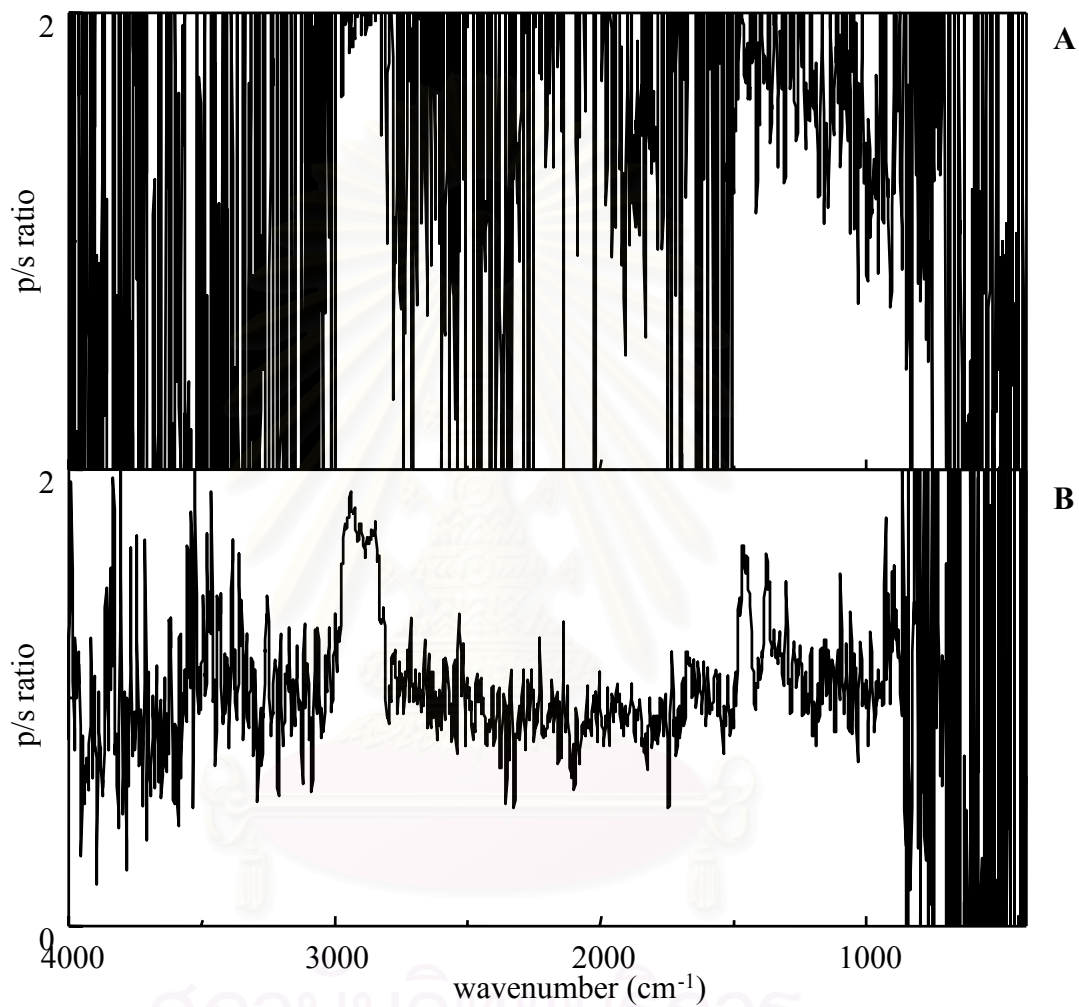


Figure 4.23 p/s ratio (A) Seagull 30° angle of incidence (B) constructed accessory 30° angle of incidence

4.2.3 Flowing of liquid

The illustration of the constructed accessory for study the flow system is shown in figure 4.24. Due to the small inlet, a liquid pump was employed in order to introduce the liquid sample into the constructed accessory. Water is utilized as sample in this experiment. Inlet and outlet pipes of the constructed accessory are made from Teflon in order to improve solvent resistance. The results indicate that, the stream of water is high turbulence. Bubbles exist inside the cell due to high power of pump and the small inlet. Moreover, the path of an infrared beam is obstructed by sample outlet. This is due to the shape of single-pass parallelepiped plate IRE. Thus the available IRE is not suitable for the flow analysis. Therefore the ATR spectra cannot collect.

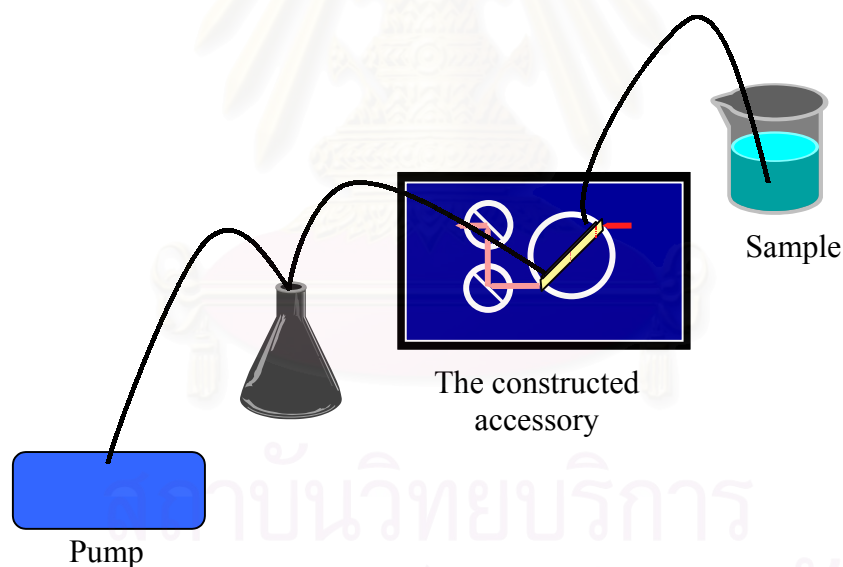


Figure 4.24 Experimental setup for study flow of liquid sample.

CHAPTER 5

CONCLUSION

The flow cell was designed and constructed with aluminium. Due to the accessory is designed for ease to operation and it is constructed with local material (high-grade aluminium), which is easy to operate, durable, and low cost. The accessory can be used with available commercial spectrometer. The gold-coated Ni-Co-Al alloy was applied as reflecting mirror in order to reduce cost and enhance light reflection. It can be fine-tune for the reflecting plane in order to enhance energy throughput.

Due to the gold-coated reflecting mirror has high reflecting efficiency, the energy throughput obtained from the constructed accessory equipped with gold-coated reflecting mirror is higher than without gold-coated reflecting mirror. The energy throughput acquired via 45° angle of incidence is higher than those acquired via 30° and 60° angle of incidence due to large aperture. The energy throughput obtained from the constructed accessory is higher than that obtained from the Baseline HATR because it can be fine-tuned on the reflecting mirror. But its is smaller than that obtained from the Seagull™ due to the number of reflections of the Seagull™ is 1.0, and the infrared beam can travel through the hemisphere shape IRE with large area. The Seagull™ has high signal to noise ratio.

In order to confirm the correction of the constructed accessory, ATR spectra of nujol of the constructed accessory were compared with commercial accessory. The peak positions of nujol acquired via the constructed accessory are the same as the Baseline HATR and the Seagull™, but its base line is smoother than that of the Baseline HATR. The signal-to-noise ratio of the constructed accessory is higher than that of the Baseline HATR. At 45° angle of incidence of the constructed accessory, ATR spectra intensity of p-polarized radiation is nearly two times of s-polarized

radiation. This observation is similar to that acquired via the Baseline HATR and nearly with the theory.

The results obtained from the constructed accessory are similar to the available commercial accessory. Therefore, the constructed accessory can be used for chemical analysis in laboratories. For flowing liquid, however, the configuration of accessory has some problems on path of light and sample outlet system due to the shape of available IRE is single-pass parallelepiped plate, which is unsuitable shape for this configuration. The problems can be solved by changing the single-pass parallelepiped (SPP) plate IRE to single-pass trapezoidal (SPT) plate IRE shape and designing newly configuration accessory for SPT plate IRE.



สถาบันวิทยบริการ
จุฬาลงกรณ์มหาวิทยาลัย

REFERENCES

1. Urban, M. W. (Ed.). (1996). Attenuated Total Reflectance Spectroscopy of Polymer: Theory and Practice, Washington, DC: American Chemical Society, pp. 3-14.
2. Harrick, N. J. (Ed.). (1979). Internal Reflection Spectroscopy, New York: Harrick Scientific Corporation, pp. 13-17, 89-109, 193-196.
3. Coleman P. B. (Ed.). (1993). Practical Sampling Techniques for Infrared Analysis, CRC Press, Inc., 55-72.
4. Hansen, W. N. (1968). Electric Fields Produced by the Propagation of Plane Coherent Electromagnetic Radiation in a Stratified Medium. *J. Opt. Soc. Am.*, 58(3), 380-390.
5. Wolf, U., Leiberich, R., and Seeba, J. (1999). Application of Infrared ATR Spectroscopy to In Situ reaction monitoring. *Catalysis Today*, 49, 411-418.
6. Harrick, N. J., Milosevic, M., and Berets, S. L., (1991). Advance in Optical Spectroscopy: The Ultra-Small Sample Analyzer. *Appl. Spectrosc.*, 45 (6), 944-948.

สถาบันวิทยบริการ
จุฬาลงกรณ์มหาวิทยาลัย



APPENDIX

สถาบันวิทยบริการ
จุฬาลงกรณ์มหาวิทยาลัย

APPENDIX A

Table A List of Internal Reflection Elements with summary of their respective uses and comments.

Type	Uses and comments
1. Single reflection IRE's 1.1 Fixed-angle IRE's-prism 1.2 Variable-angle IRE's 1.2.1 Hemicylinder 1.2.2 Microhemicylinder 1.2.3 Hemisphere	Strongly absorbing liquids, solids, and pastes. Same as prisms-in addition, optical constants, also useful to control spectral contrast. Small samples and minute quantities, Angle of incidence is not well defined in these IRE's
2. Multiple reflection IRE's 2.1 Fixed-angle multiple reflection plates 2.1.1 Single-pass plate 2.1.2 Double-pass plate 2.1.3 Vertical double-pass plate 2.1.4 Multiple-pass internal reflection plate 2.1.5 Single-pass, double-sampling plate 2.1.6 Double-pass, double-sampling plate 2.2 Variable-angle multiple reflection plates 2.2.1 Single-pass plate 2.2.2 Double-pass plate 2.2.3 Vertical double-pass plate	Weakly absorbing bulk and thin films; very thin films and surface studies. Surface studies, vacuum studies, liquids and powders. Simplifies instrumentation but output power level may be lower than for single-pass plate. Liquids and powders. Folded system for many reflections. Has twice the sensitivity of other plates. All single, double, and multiple-pass plates can be converted into variable-angle plates by providing quarter rounds at entrance and exit apertures. In addition to the uses of the fixed-angle plates, these can be used for measuring optical constants and study of interaction mechanisms at reflecting surfaces. These are complicated structures and should be used only when necessary.

Type	Uses and comments
2.3 Unipoint multiple internal reflection element	
2.3.1 Optical cavity	Useful for very weak absorbers and very minute quantities. It is a fixed wavelength IRE.
2.3.2 Rosette	Minute quantities- a complex structure and requires precision alignment.
2.4 Other geometries	
2.4.1 Modified hemicylinder	Same as hemicylinder but employs a few reflections (3 to 5). Can be used over only limited angular range.
2.4.2 V-shaped IRE	Liquids and solids. This IRE can be placed in sampling space and requires no additional instrumentation.
2.4.3 Cylindrical rods and fibers	Simple to make but complicates optics.

Appendix B

Source codes of spectral simulation for generate refractive index (n) and absorption index (k).

Input file for generate n and k

% Enter input data

```

file_out = 'Film.' ; % output filename with dot '.'
wns     = 4000 ; % started wave number (cm-1)
wne     = 400 ; % ended wave number (cm-1)
res     = -2 ; % resolution of wave number (cm-1)
N_INF   = 1.5 ; %dielectric function at infinite wave number(no absorption)
NP      = 5 ; % number of peaks
PP      = [3000 2500 2000 1500 1000] %peak position or band center (cm-1)
K_MAX   = [0.05 0.05 0.05 0.05 0.05] ; % peak intensity(height) in terms of k_max
HWHH    = [10 10 10 10 10] ; % Half-Width at Half-Height
%-----

```

สถาบันวิทยบริการ
จุฬาลงกรณ์มหาวิทยาลัย

Calculating file for generate n and k

```

%-----
% Start running program for generating n and k spectra ...
%-----

global N_INF NP PP K_MAX HWHH

Input_nk ; % Import input data (Input_nk)
wn=((wns:res:wne)');
%HWHH=FWHH./2; % Beware yourself about Input data!HWHH or FWHH
[n,k]=Eq_nk(wn);

if NP<=0 ;
    error('Number of peak must be POSITIVE INTEGER !!')
end
%-----
% Write calculated data to ascii output file
%-----
fwriteid=fopen(strrep(file_out,'!','n'),'w') ;
fprintf(fwriteid,'%10.2f %12.6f\n',[wn n]) ;
status=fclose(fwriteid) ;
fwriteid=fopen(strrep(file_out,'!','k'),'w') ;
fprintf(fwriteid,'%10.2f %12.6f\n',[wn k]) ;
status=fclose(fwriteid) ;
%-----
% Read calculated data on screen
%-----
%frid=fopen(strrep(file_out,'!','nk'),'r') ;
%data=(fscanf(frid,'%g %g %g',[3,inf]))'
%fclose(frid) ;
%disp(' wave number      n      k  ')

```



```
%-----  
%Plot n and k spectra in the same window  
%-----  
clf;  
subplot(2,1,1); plot(wn,n);  
title ('refractive index n');  
subplot(2,1,2); plot(wn,k);  
title ('absorption index k');  
xlabel('wavenumber (cm-1)');  
  
disp('Finish all instructions!!')  
%-----
```



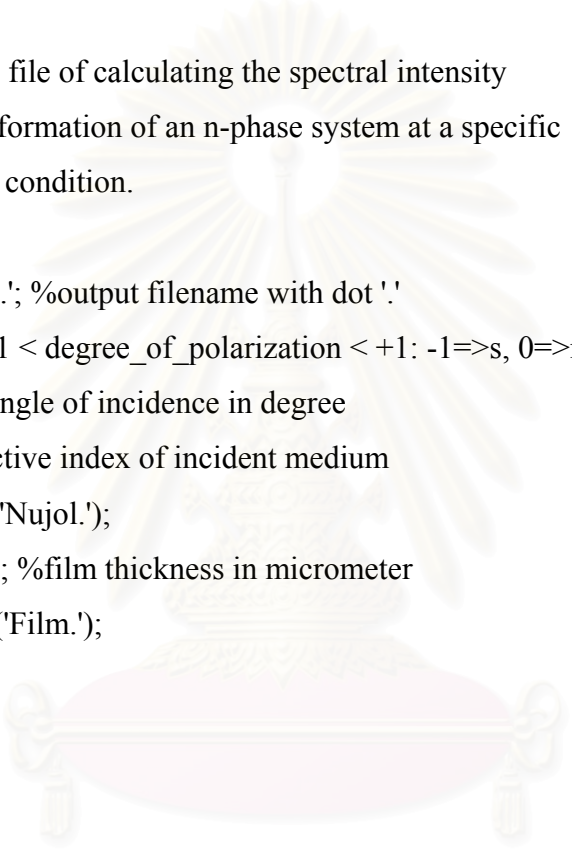
สถาบันวิทยบริการ
จุฬาลงกรณ์มหาวิทยาลัย

Appendix C

Source codes of spectral simulation for simulate spectrum of nujol.

Input file for simulate spectra

```
%This is a data file of calculating the spectral intensity
%and related information of an n-phase system at a specific
%experimental condition.
%
file_out='Nujol.'; %output filename with dot '.'
polarize=0; %-1 < degree_of_polarization < +1: -1=>s, 0=>non, 1=>p
t0=45; %start angle of incidence in degree
n0=4.0; %refractive index of incident medium
file_film=char('Nujol.');
```



```
film_thic=[3.0]; %film thickness in micrometer
file_subs=char('Film.');
```

สถาบันวิทยบริการ
จุฬาลงกรณ์มหาวิทยาลัย

Calculating file for simulate spectra

```
%This program is for Spectral Simulation
```

```
%
```

```
clear;
```

```
global Rp Tp Rs Ts
```

```
Spect_Sim_Data;%load Substrate n and k
```

```
temp=load(strrep(file_subs,',''.n'));
```

```
wn=temp(:,1);
```

```
ns=temp(:,2);
```

```
temp=load(strrep(file_subs,',''.k'));
```

```
w0=temp(:,1);
```

```
ks=temp(:,2);
```

```
test_resolution(wn,w0);%load Film n and k
```

```
n1=[];
```

```
k1=[];
```

```
for i = 1:size(file_film,1)
```

```
    temp=load(strrep(file_film(i,),''.n'));
```

```
    n1=[n1 temp(:,2)];
```

```
    w0=temp(:,1);
```

```
    test_resolution(wn,w0);
```

```
    temp=load(strrep(file_film(i,),''.k'));
```

```
    k1=[k1 temp(:,2)];
```

```
    %k1=linspace(0,0,1801);
```

```
    w0=temp(:,1);
```

```
    test_resolution(wn,w0);
```

```
end
```

```
%Start spectral simulation
```

```
RpnP=[];
```

```
RsnP=[];
```

```

TpnP=[];
TsnP=[];
t0=deg2rad(t0); %convert angle(degree) into angle(radian)
for j=1:size(wn,1)
    wnj=wn(j,1);
    nk=complex(n1(j,:) ,k1(j,:));
    nks=complex(ns(j,1) ,ks(j,1));
    nPhase_Hansen(wnj,t0,n0,nk,nks,film_thic)
    RpnP=[RpnP,Rp];
    RsnP=[RsnP,Rs];
    TpnP=[TpnP,Tp];
    TsnP=[TsnP,Ts];
end

%graphic output of the simulation
clf;
Rn=(RsnP+RpnP)/2;
Abs_Rn=-log(Rn);
subplot(2,2,1); plot(wn,Abs_Rn);
axis([400 4000 0 0.2]);
xlabel('wavenumber');
ylabel('absorbance');
Abs_Rs=-log(RsnP);
subplot(2,2,2); plot(wn,Abs_Rs);
axis([400 4000 0 0.2]);
xlabel('wavenumber');
ylabel('s-absorbance');
Abs_Rp=-log(RpnP);
subplot(2,2,3); plot(wn,Abs_Rp);
axis([400 4000 0 0.2]);
xlabel('wavenumber');
ylabel('p-absorbance');

```

```
Ratio=(Abs_Rp/Abs_Rs);  
subplot(2,2,4); plot(wn,Ratio);  
axis([400 4000 0 3]);  
xlabel('wavenumber');  
ylabel('ratio');
```

```
%ASCII format output  
file=strrep(file_out,'!','Abs_n');  
Dn=[wn Abs_Rn'];  
dlmwrite(file,[Dn],'\t');  
file=strrep(file_out,'!','Abs_s');  
Ds=[wn Abs_Rs'];  
dlmwrite(file,[Ds],'\t');  
file=strrep(file_out,'!','Abs_p');  
Dp=[wn Abs_Rp'];  
dlmwrite(file,[Dp],'\t');
```

disp('Finish')

สถาบันวิทยบริการ
จุฬาลงกรณ์มหาวิทยาลัย

CURRICULUM VITAE

Songsak Tepakakorn

- 1976 Born October 17th, in Chonburi, Thailand
- 1982-1988 Elementary School (Mareimmaculate convent)
- 1988-1991 Primary School (Chonradsadonumrung School, Chonburi)
- 1991-1994 High School (Chonradsadonumrung School, Chonburi)
- 1994-1998 Bachelor degree at Department of Chemistry, Faculty of Science, Burapha University, Chonburi
- 1998-2001 Master degree student at Department of Chemistry, Faculty of Science, Chulalongkorn University, Bangkok

สถาบันวิทยบริการ
จุฬาลงกรณ์มหาวิทยาลัย